

<b>Titre:</b> Title:	Preparation of Highly Exfoliated Polyester–Clay Nanocomposites: Process–Property Correlations
<b>Auteurs:</b> Authors:	Hamid Dalir, Rouhollah D. Farahani, Vireya Nhim, Benjamin Samson, Martin Lévesque et Daniel Therriault
<b>Date:</b>	2012
<b>Type:</b>	Article de revue / Journal article
<b>Référence:</b> Citation:	Dalir, H., Farahani, R. D., Nhim, V., Samson, B., Lévesque, M. & Therriault, D. (2012). Preparation of Highly Exfoliated Polyester–Clay Nanocomposites: Process–Property Correlations. <i>Langmuir</i> , 28(1), p. 791-803. doi: <a href="https://doi.org/10.1021/la203331h">10.1021/la203331h</a>

 **Document en libre accès dans PolyPublie**

Open Access document in PolyPublie

<b>URL de PolyPublie:</b> PolyPublie URL:	<a href="https://publications.polymtl.ca/10385/">https://publications.polymtl.ca/10385/</a>
<b>Version:</b>	Version finale avant publication / Accepted version Révisé par les pairs / Refereed
<b>Conditions d'utilisation:</b> Terms of Use:	Tous droits réservés / All rights reserved

 **Document publié chez l'éditeur officiel**

Document issued by the official publisher

<b>Titre de la revue:</b> Journal Title:	Langmuir (vol. 28, no 1)
<b>Maison d'édition:</b> Publisher:	ACS
<b>URL officiel:</b> Official URL:	<a href="https://doi.org/10.1021/la203331h">https://doi.org/10.1021/la203331h</a>
<b>Mention légale:</b> Legal notice:	This document is the Accepted Manuscript version of a Published Work that appeared in final form in Langmuir, copyright © [copyright © 2012, American Chemical Society] after peer review and technical editing by the publisher. To access the final edited and published work see <a href="https://doi.org/10.1021/la203331h">https://doi.org/10.1021/la203331h</a>

**Ce fichier a été téléchargé à partir de PolyPublie,  
le dépôt institutionnel de Polytechnique Montréal**

This file has been downloaded from PolyPublie, the  
institutional repository of Polytechnique Montréal

<http://publications.polymtl.ca>

1  
2  
3  
4  
5  
6  
7  
8  
9  
10  
11  
12  
13  
14  
15  
16  
17  
18  
19  
20  
21  
22  
23  
24  
25  
26  
27  
28  
29  
30  
31  
32  
33  
34  
35  
36  
37  
38  
39  
40  
41  
42

# Preparation of highly exfoliated polyester-clay nanocomposites: process-property correlations

43  
44  
45  
46  
47  
48  
49  
50  
51  
52  
53  
54  
55  
56  
57  
58  
59  
60

*Hamid Dalir, Rouhollah D. Farahani, Vireya Nhim, Benjamin Samson, Martin Lévesque and*

*Daniel Therriault\**

Center for Applied Research on Polymers and Composites (CREPEC), Department of Mechanical  
Engineering, École Polytechnique de Montréal.

\* Corresponding author.

Phone: 1 (514) 340-4711 (ext. 4419).

Mailing address: C.P. 6079, Succ. Centre-ville, Montréal, QC H3C 3A7, CANADA.

E-mail address: [daniel.therriault@polymtl.ca](mailto:daniel.therriault@polymtl.ca) (D. Therriault).

**ABSTRACT**

1  
2  
3  
4 A large number of polyester nanocomposite batches featuring different kinds of nanoclay surface  
5 modifiers and up to 6 wt.% nanoclay were manufactured using a solvent-based technique.  
6  
7 Montmorillonite platelets modified with ammonium ions of different chemical architectures were  
8  
9 examined in order to study the effect of ammonium ions on the extent of surface reactions with long  
10  
11 chain fatty acids. The ammonium montmorillonite was first dispersed and suspended in acetone. This  
12  
13 suspension was further esterificated with dotriacontanoic (lacceroic) acid to form high density brushes  
14  
15 on the clay surface. This led to achieving higher basal plane spacing of the montmorillonite platelets  
16  
17 owing to the reduction of electrostatic interactions holding them. The outcome of the surface  
18  
19 esterification was analyzed by Fourier transform infrared spectroscopy (FTIR) and X-ray diffraction  
20  
21 (XRD). The esterificated ammonium modified clays were then mixed by five different mixing strategies  
22  
23 based on the use of a three-roll mill mixer (TRM) and/or ultrasonication (US) in order to obtain the  
24  
25 desired polyester-nanoclay dispersion, intercalation, and exfoliation. The dispersion states of the  
26  
27 modified nanoclay in polymer were characterized from XRD, scanning electron microscopy (SEM), and  
28  
29 low and high magnification transmission electron microscopy (TEM). Mechanical, thermal and barrier  
30  
31 properties of the resulting composites were experimentally characterized. The Mori-Tanaka method  
32  
33 along with an orientation distribution function was used to verify the experimental effective stiffness of  
34  
35 the polyester nanocomposite systems. The aspect ratio of nanoclays and their level of intercalation  
36  
37 and/or exfoliation after mixing were also confirmed by the comparison of the experimental diffusivity  
38  
39 results with those of Fick's diffusion model. Systems having 4 and 6 wt.% esterificated ammonium  
40  
41 nanoclay and prepared according to a combined TRM/US mixing procedure showed optimal  
42  
43 performance with balanced properties and processing ease, thereby showing potential for use in  
44  
45 automotive, transportation and packaging industry.  
46  
47  
48  
49  
50  
51  
52  
53  
54  
55  
56  
57  
58  
59  
60

## 1. Introduction

1  
2  
3  
4  
5 Polymer-clay nanocomposite (PCN) is a class of materials consisting of either thermosets,  
6 thermoplastics, rubbers or co-polymers as the matrix and nanoclay as the reinforcement.<sup>1,2</sup>  
7  
8 Montmorillonite layered-silicate smectite consists of stacks of 1 nm thick aluminosilicate layers or  
9 platelets regularly spaced. Each layer consists of a central Al-octahedral sheet fused to two tetrahedral  
10 silicate sheets. Isomorphic substitutions of aluminum by magnesium in the octahedral sheet generate  
11 negative charges, which are compensated for by alkaline earth- or hydrated alkali-metal cations.<sup>3,4</sup> The  
12 electrostatic and van der Waals forces holding the layers together are relatively weak in these  
13 montmorillonites and the interlayer distance varies depending on the radius of the cation present and its  
14 degree of hydration. The easy swelling of high aspect ratio platelets in water makes them suitable  
15 substrates for surface ion exchange with alkyl ammonium ions. This modifies the surface so as to make  
16 them compatible with organic polymer matrices to achieve their exfoliation.<sup>5,6</sup> The exfoliation of  
17 conventional ammonium ion modified clays in polar matrices has been successfully achieved owing to  
18 positive interactions between the matrix and polar clay interlayers. On the other hand, these ammonium  
19 ion modified montmorillonites have been at best partially exfoliated or marginally intercalated when  
20 non-polar matrices, like polyethylene and polypropylene are used which is due to the absence of any  
21 interactions. The extent of exfoliation in these non-polar matrices was observed to enhance when chain  
22 density of the ammonium ion attached on the surface or the length of the alkyl chains were increased  
23 due to resulting decrease in electrostatic interactions between the clay platelets.<sup>7,8</sup> But, the limit of  
24 solubility as well as steric hindrance at the surface limits the exchange of pre-formed “big” molecules  
25 on the surface. Physical adsorption of polar molecules on the surfaces of ammonium modified  
26 montmorillonites can be one way to balance the residual electrostatic forces in the platelets. However,  
27 the risk of these molecules being pulled out during heat treatment or cleaning is higher. Polarization of  
28 matrices to improve their interactions with clay interlayers has also been commonly attempted by  
29 compatibilizers, but the extent of polarization may limit the mechanical performance of the  
30  
31  
32  
33  
34  
35  
36  
37  
38  
39  
40  
41  
42  
43  
44  
45  
46  
47  
48  
49  
50  
51  
52  
53  
54  
55  
56  
57  
58  
59  
60

1  
2  
3  
4  
5  
6  
7  
8  
9  
10  
11  
12  
13  
14  
15  
16  
17  
18  
19  
20  
21  
22  
23  
24  
25  
26  
27  
28  
29  
30  
31  
32  
33  
34  
35  
36  
37  
38  
39  
40  
41  
42  
43  
44  
45  
46  
47  
48  
49  
50  
51  
52  
53  
54  
55  
56  
57  
58  
59  
60  
composites.<sup>9-11</sup> Ideally, if the ammonium ions with reactive groups are exchanged first on surface and are then subsequently reacted to attach further long chains, high density brushes with long resulting alkyl chains chemically bound to the surface can be generated.<sup>12-18</sup>

PCN has recently received considerable attention, both from academia and the industry, due to their potential enhancement in physical properties such as mechanical properties (e.g., mechanical strength<sup>19</sup>, hardness<sup>20</sup>, abrasion resistance<sup>21</sup>), thermal properties (e.g., thermal stability<sup>22</sup>, flame retardant<sup>23</sup>, thermal conductivity<sup>24</sup>), barrier properties (e.g., gas barrier<sup>25</sup>, pervaporation<sup>26</sup>), electro-rheological properties<sup>27</sup> and corrosion protection properties<sup>28</sup> compared to the plain polymer. The thermo-mechanical responses of polymers are favorably altered by the addition of a trace amount of nanofillers. To obtain optimal nanocomposite properties, the following four structural parameters should be maximized: (1) the particle aspect ratio, (2) particle dispersion, (3) particle packing (or alignment), and (4) polymer to particle interfacial stress transfer.<sup>29-33</sup>

Nanoclay particles can be used to reduce the diffusion and permeation of molecules through the polymer matrix.<sup>34-36</sup> The type and content of clay particle, and its compatibility with the host matrix greatly influence the permeability of the membrane. Drozdov et al.<sup>37</sup> showed that the diffusivity deteriorates with higher clay content. The diffusion of molecules and its kinetics, through nanoclay-based nanocomposites were also examined by many researchers<sup>38-40</sup> and a substantial decrease in moisture permeability in comparison with those of virgin polymer matrix was reported. The reduction in permeability was attributed to the extremely high aspect ratio of clay platelets, which increased the tortuosity of the diffusion path of the molecules into the nanocomposite.

The addition of clay in the polyester matrix usually leads to three different microstructures depending on the nature of the material and the method of preparation.<sup>41-48</sup> When the polyester is unable to intercalate between the silicate sheets, a phase separated composite is obtained in which the materials stay in the same range as traditional microcomposites. Intercalated structure, in which a single (or more) polymer chain intercalated between the silicate layers results in a well ordered multilayer morphology

1 built up with alternating polymeric and inorganic layers. When the silicate layers are completely and  
2 uniformly dispersed in the continuous polyester matrix, an exfoliated or delaminated structure is  
3 obtained. The intercalated and exfoliated structures are formed only when the clay is organically treated  
4 with surfactants.<sup>36,42</sup>  
5  
6  
7  
8  
9

10 In this study, we prepared polyester polymer-nanoclay nanocomposites in acetone by the use of  
11 esterificated ammonium modified nanoclays. Esterification with long alkyl chains led to achieving  
12 higher clay basal spacing in order to decrease the electrostatic interactions to ease the clay exfoliation in  
13 the polymer matrix system. The increase in the organic matter present on the clay surface due to  
14 esterification was characterized by FTIR and XRD. The Mori-Tanaka method and the Fick's diffusion  
15 model were used to predict the effective stiffness and diffusivity behavior of these polyester-based  
16 nanocomposites, respectively. The following sections summarize an experimental evaluation of the  
17 polyester-nanoclay composites with details on the processing method, characterization of the nanoclay  
18 morphology and distribution, mechanical, thermal and diffusivity testing, and the optimization of the  
19 nanocomposite behavior.  
20  
21  
22  
23  
24  
25  
26  
27  
28  
29  
30  
31  
32  
33  
34

## 35 **2. Experimental Methods**

### 36 ***2.1. Materials and nanocomposite preparation***

37  
38  
39  
40  
41  
42 The nanocomposite material was a mixture of one of the three different types of esterificated  
43 predispersed nanoclays (Cloisite® 11B, Cloisite® 15A, and Cloisite® 30B, Southern Clay Products,  
44 Louisville, USA), with different surface modifiers as listed in Table 1. A catalyst cured thermosetting  
45 polyester (RL7520, Progress Plastiques Cie, Drummondville, CAN) having a viscosity of 200 mPa.s,  
46 gel time of 75 min, tensile modulus of 3.6 GPa, and ultimate tensile strength of 80 MPa was used with  
47 NOROX® MEKP-9 (NORAC Inc., California, USA) as the catalyst. The desired amount of nanoclay  
48 (either 2, 4, or 6 wt.%) was first dispersed in acetone 99.9% and dotriacontanoic (lacceroic) acid  
49 (Sigma-Aldrich Ltd., Ontario, CAN) solution followed by 4-(dimethylamino)pyridine (DMAP) and  
50  
51  
52  
53  
54  
55  
56  
57  
58  
59  
60

1 diisopropylcarbodiimide (DIC) procured from Sigma-Aldrich Ltd. (Ontario, CAN) to achieve higher  
2 basal plane spacing of the montmorillonite platelets. After ultrasonication (ultrasonic cleaner 8891,  
3 Cole-Parmer) at 42 kHz for 1 h, clay resuspension was done in dimethylformamide (DMF) from Sigma-  
4 Aldrich Ltd. (Ontario, CAN). Then the polyester was slowly added to the solution over a stirring hot  
5 plate (model SP131825, Barnstead international). The samples were further mixed by investigating five  
6 different mixing strategies resulting in an array of several polyester nanocomposite experimental  
7 batches listed in Table. 1.  
8  
9  
10  
11  
12  
13  
14  
15  
16  
17

## 18 ***2.2. Esterification of ammonium modified nanoclays***

19  
20  
21 For the surface esterification reactions, 0.5 g of modified clay was suspended in 5 mL of acetone.  
22 The suspension was sonicated twice for 10 min while keeping cold to avoid solvent evaporation.  
23 Dotriacontanoic acid (acid/clay mole ratio of 5.0) was then added to the clay followed by DMAP  
24 (acid/DMAP mole ratio of 0.05). The contents were then stirred by addition of DIC (DIC/acid mole  
25 ratio of 1.2) for 24 h at room temperature. The resulting thick gel was filtered to remove the unreacted  
26 acid and other reagents along with the solvent-soluble urea formed during the esterification reaction.  
27 The filtrate was added with ether in order to precipitate the urea formed during the reaction to confirm  
28 the surface reaction. The reacted clay was resuspended in DMF followed by sonication and was filtered  
29 and dried under vacuum at 90 °C.  
30  
31  
32  
33  
34  
35  
36  
37  
38  
39  
40  
41  
42

## 43 ***2.3. Nanocomposite mixing strategies and nomenclature***

44  
45  
46 Figure 1 shows a schematic representation of the five mixing strategies. In strategy I, Styrene (ST,  
47  $C_6H_5CH=CH_2$ , Sigma-Aldrich Ltd., Ontario, CAN) and catalyst (CA) were added to the mixture and  
48 then only ultrasonicated (US) for 30 min. In strategies II and III, the nanocomposite mixtures were  
49 passed several times through a three-roll mixing mill (TRM, Exakt 80E, Exakt Technologies Inc.) where  
50  
51  
52  
53  
54  
55  
56  
57  
58  
59  
60

**Table 1.** Experimental matrix showing nanoclay specifications and specimen batch numbers according to different mixing strategies and variation in nanoclay contents.

Nanoclay type	Molecular structure	Surface modifier	Concentration	Moisture (%)	Nanoclay content (wt.%)	Batch number				
						Mixing strategy				
						I	II	III	IV	V
Cloisite® 11B	$\begin{array}{c} \text{CH}_3 \\   \\ \text{CH}_3 - \text{N}^+ - \text{CH}_2 - \text{C}_6\text{H}_5 \\   \\ \text{HT} \end{array}$	2MBHT	95 meq/100g	> 4%	2	1	2	3	4	5
					4	6	7	8	9	10
					6	11	12	13	14	15
Cloisite® 15A	$\begin{array}{c} \text{CH}_3 \\   \\ \text{CH}_3 - \text{N}^+ - \text{HT} \\   \\ \text{HT} \end{array}$	2M2HT	125 meq/100g	> 2%	2	16	17	18	19	20
					4	21	22	23	24	25
					6	26	27	28	29	30
Cloisite® 30B	$\begin{array}{c} \text{CH}_2 \text{CH}_2\text{OH} \\   \\ \text{CH}_3 - \text{N}^+ - \text{T} \\   \\ \text{CH}_2 \text{CH}_2\text{OH} \end{array}$	MT2EtOH	90 meq/100g	> 2%	2	31	32	33	34	35
					4	36	37	38	39	40
					6	41	42	43	44	45



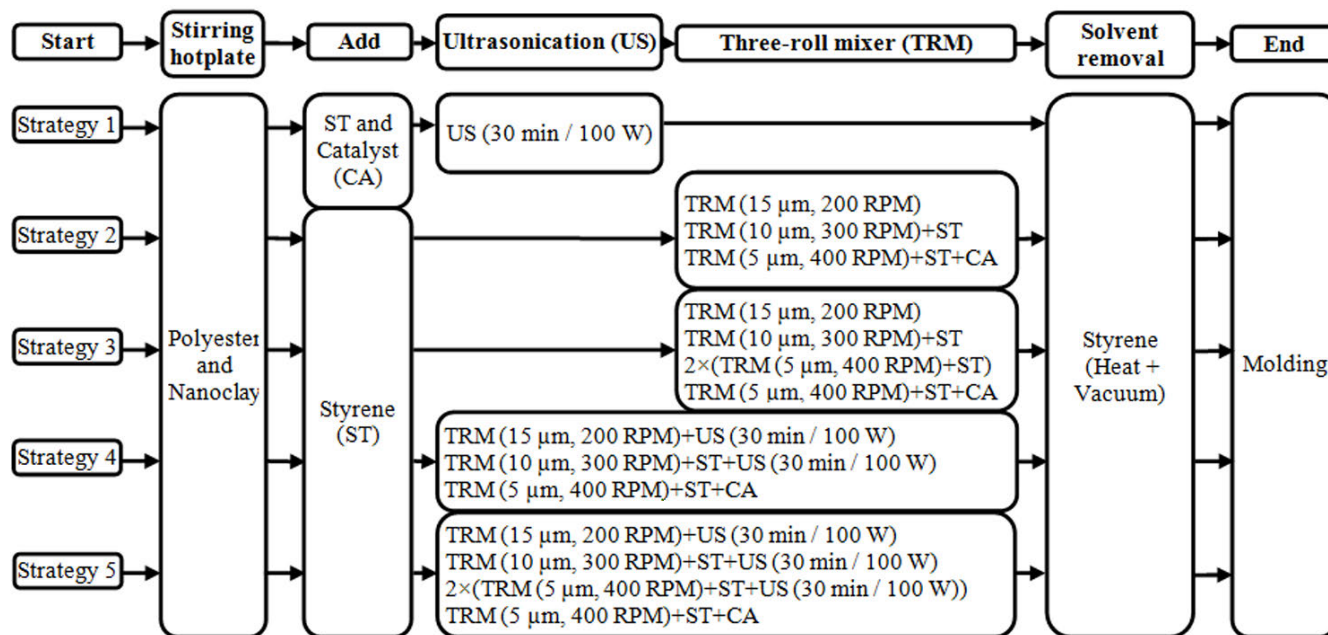


**Figure 1.** Processing of esterificated nanoclay reinforced polyester-based nanocomposites.

the gap between the rolls and the speed of the apron roll were adjusted at 15  $\mu\text{m}$ -200 RPM, 10  $\mu\text{m}$ -300 RPM and either one or three times at 5  $\mu\text{m}$ -400 RPM, for three or five passes, respectively. For strategies IV and V, the same procedure and parameters as those of strategies II and III were chosen, respectively, however US was performed after each TRM process, except for the last pass. These five mixing strategies were repeated for three concentrations (2, 4, and 6 wt.%) of the three modified clays. The obtained esterificated nanoclay-polyester mixtures were then immediately degassed for  $\sim 30$  min and poured into tensile test sample molds (ASTM D638) and placed under vacuum for  $\sim 6$  h at room temperature for complete solvent evaporation.

The nomenclature used to describe the nanocomposite is: "A/B/C", where "A" and "B" represent the type and the content of cloisite®, respectively. "C" refers to the selected mixing strategy number. For example, batch number 24 in Table 1 is referred to as 15A/4/IV, indicating the mixing of 100 g of resin system with 4.167 g (4 wt.%) of esterificated Cloisite® 15A nanoclay platelets according to strategy IV.

## 2.4. Testing and characterization

FTIR spectrums (VECTOR 22, Bruker Optics Inc.) of the surface treated nanoclays were obtained by preparing their pill shape samples in KBr. The degree of intercalation and exfoliation was analyzed based on scanning electron microscope (SEM, JEOL JSM-7600TFE), transmission electron microscope (TEM JEOL JEM-2100F) images and X-ray diffraction (XRD, X'Pert PRO Diffractometer). The interlayer separation measurements were carried out with Pro X-ray diffractometer with Cu target and Ni filter at a scanning rate of 2°/min, with CuK $\alpha$  radiation ( $\lambda_w = 1.541 \text{ \AA}$ ) operating at 30 kV and 15 mA. Tensile tests were carried out using tensile test machine (MTS 810) with a 25 kN load cell at the crosshead speed of 1 mm/min (ASTM D638). A minimum of five tensile specimens were tested for each nanocomposite system. Dynamic mechanical thermal analyses (DMTA) were only performed on the specimens showing the most promising properties (i.e., specimens with batch numbers 4, 9, 14, 19, 24, 29, 34, 39 and 44 (Table 1)). The linear coefficient of thermal expansion (CTE) above and below the glass transition temperature ( $T_g$ ) was obtained by thermo-mechanical analysis using a TA Instruments DMA 2980. The samples were heated from room temperature to 140 °C at a rate of 4 °C/min. The axial strain and temperature were measured throughout the test. The linear slope of the strain-temperature curve is reported as the CTE. The  $T_g$  was obtained from the intersection of the two linear portions of the strain-temperature curve. Moisture absorption testing was performed using a Cole Parmer oven that allows immersion of samples in a distilled water bath with temperature maintained at 50 °C according to ASTM D570-98. The nanocomposites samples used for moisture measurements were rectangular bars of  $\sim 60 \text{ mm} \times 12 \text{ mm} \times 3 \text{ mm}$  coated with polyurethane (NEA123MB, Norland Products) on all edges to reduce edge effects and constraint the diffusion to occur mainly through the thickness of the sample. All samples were polished to ensure flat and parallel surfaces. The polished samples were placed in a vacuum oven at 80 °C for 24 h to remove residual moisture. After water immersion, the weight of the samples was measured every 8 h for the first 4 days, followed by once a day until steady state condition

1 was achieved. Moisture diffusivity coefficients were obtained from the moisture gain versus time plots  
2  
3 for various polyester-based nanocomposites.  
4  
5

### 6 **3. Results**

7  
8

9  
10 Several nanocomposite systems (Table 1) were characterized with different mixing strategy and  
11 nanoclay type and content. Depending on the property studied, experimental results showed different  
12 levels of variation. This is to be expected, as nanocomposite materials have several sources for  
13 variation, such as multiple heterogeneities (e.g., nanoclay, styrene), processing parameters (e.g., degree  
14 of sonication, residual acetone), and their effect is different for each parameter characterized. In the  
15 following sections, the summary and observations on different properties are interpreted by considering  
16 the salient features of the average experimental data. The virgin polyester corresponds to 0% nanoclay  
17 content and is considered as the baseline material system.  
18  
19  
20  
21  
22  
23  
24  
25  
26  
27  
28

#### 29 ***3.1. Nanoclay basal spacing enhancement by their surface treatments***

30  
31

32  
33 Esterification of the clay platelets to improve their exfoliation potential when sheared in non-polar  
34 polyesters, generates brushes which are not only bound ionically to the surface, but also have desired  
35 chain lengths. Quaternary ammonium ions with varying number of reactive groups can be initially  
36 exchanged to the surface and the subsequent surface reactions can help to generate varying densities of  
37 the alkyl chains on the surface. Figure 2 shows the reaction scheme of dotriacontanoic acid with  
38 dimethyl(dihydrogenatedtallow)ammonium (2M2HT) modified montmorillonite. Although the presence  
39 of carboxyl groups can lead to further enhancement of polarity in the clay interlayers, however, the  
40 attachment of long alkyl chains can impart enough non-polar character in the interlayer as well as  
41 distance separating the platelets thus reducing the interactions between them.  
42  
43  
44  
45  
46  
47  
48  
49  
50  
51  
52  
53  
54

55 The evidence for the esterification of the ammonium modified clay platelets with dotriacontanoic  
56 acid comes from FTIR studies with a  $2\text{ cm}^{-1}$  resolution in a wave-number ranging from  $4000$  to  $400\text{ cm}^{-1}$   
57  
58  
59  
60

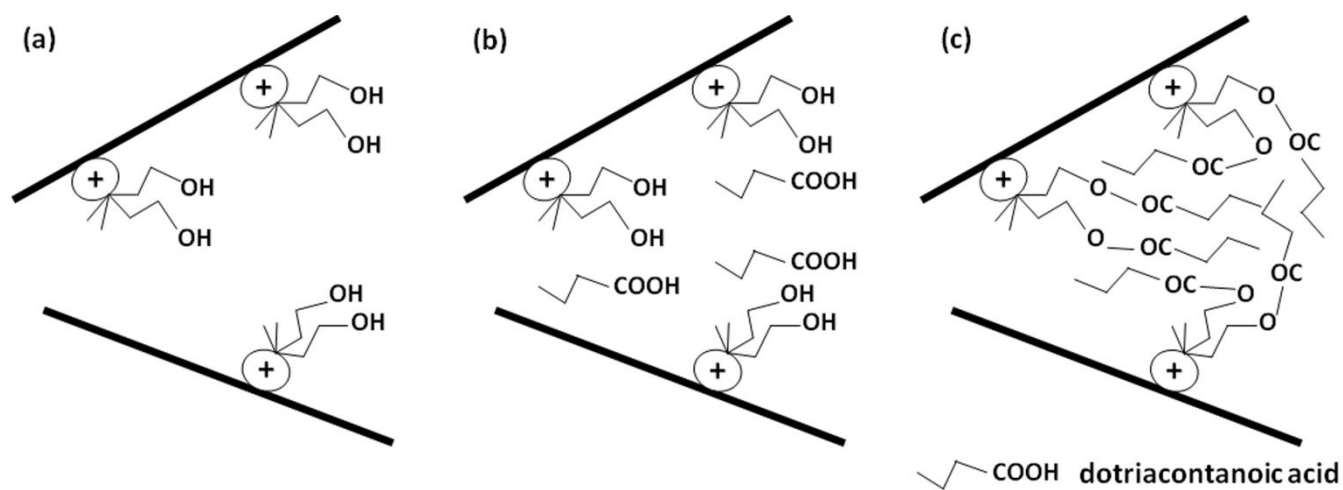


**Figure 2.** Schematic of surface esterification reaction of montmorillonite modified with 2M2HT with dotriacontanoic acid: (a) the ammonium modified clay platelets, (b) the addition of dotriacontanoic acid, (c) the formation of long alkyl chains.

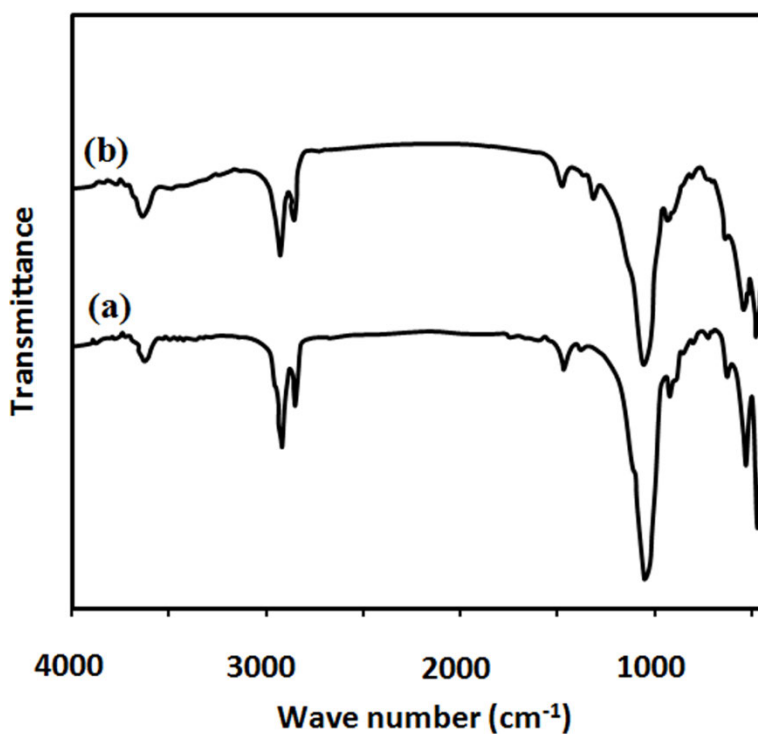


**Figure 3.** FTIR spectra of ammonium modified clay platelets (a) before, and (b) after esterification with dotriacontanoic acid.

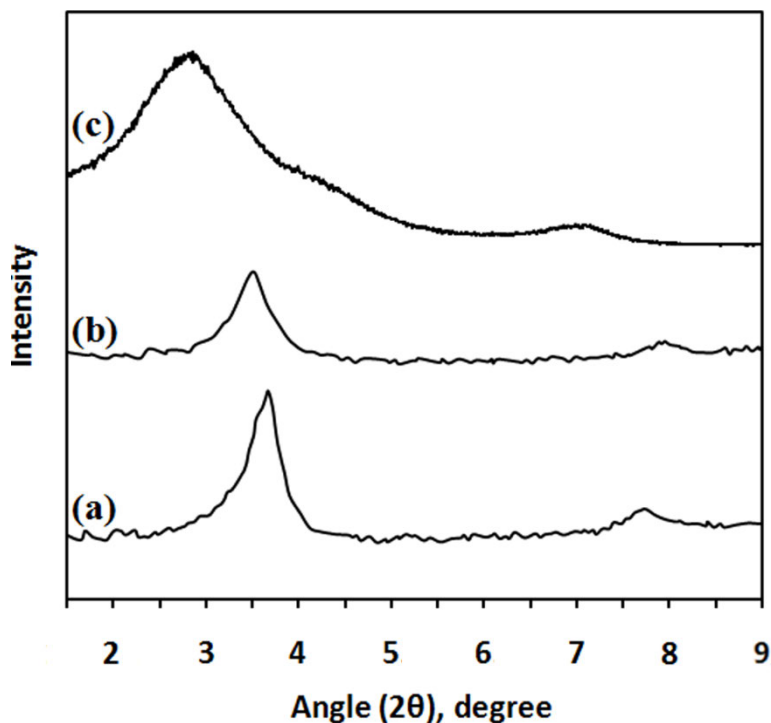


**Figure 4.** XRD diagrams of (a) ammonium modified clays, (b) precipitated ammonium modified clays in acetone, and (c) alkyl chain grafted ammonium modified clays.

with 20 scans. The FTIR spectrum of the ammonium modified clay platelets (curve (a) of Figure 3) displays typical  $\text{-OH}$  stretching absorbencies at  $3634\text{ cm}^{-1}$ .<sup>49</sup> From  $3000$  to  $2800\text{ cm}^{-1}$ , the typical  $\text{CH}_2$  stretching band of the ammonium surfactant appears. Between  $1480$  and  $1450\text{ cm}^{-1}$ , the  $\text{CH}_2$  band for symmetric bending or scissoring mode becomes evident.  $\text{CH}_2$  small bands are also seen from  $740$  to  $710\text{ cm}^{-1}$ . The bands at  $1035$ , and  $914\text{ cm}^{-1}$  can be collectively attributed to  $\text{Si-O}$  stretching vibrations.<sup>50</sup> The peaks at  $875$  and  $836\text{ cm}^{-1}$  could be attributed to  $\text{AlFeOH}$  and  $\text{AlMgOH}$  bending vibrations, respectively.<sup>51</sup> The spectrum of the esterificated clay platelets displays almost the same pattern as that of ammonium modified clay except for a new band of  $\text{O-OC}$  stretching at  $1313\text{ cm}^{-1}$ , which indicates the grafting of the alkyl chains to the ammonium organic groups on the clay mineral surface.

The change of morphology of clay during each stage of processing was also monitored using XRD. The XRD diagrams of the ammonium modified clays, precipitated ammonium modified clays in acetone, as well as alkyl chain grafted ammonium modified clays are collected in Figure 4. For

Cloisite® 15A, a peak was observed at 3.59° (curve (a)) which was shifted to 3.50° (curve (b)) when suspended in acetone. When the clay-acetone suspension was mixed with dotriacontanoic acid, the peak was shifted to a lower peak at 2.95°. The interlayer distance ( $d$ -spacing) of clays inside the nanocomposites is obtained from Bragg's law:<sup>41,42</sup>

$$2d\sin\theta = n\lambda_w, \quad (1)$$

where  $d$  is the interlayer distance of clay,  $\lambda_w$  is the wavelength used,  $n$  is the order which is equal to 1 for the first order, and  $\theta$  is the measured angle. Therefore, the  $d$ -spacing of the Cloisite® 15A is measured about 24.6 Å which is increased to 25.2 Å when suspended in acetone indicating a slightly exfoliated structure and to 29.9 Å (~ 20% improvement) for the alkyl chain grafted clays. The basal spacing increases of Cloisite® 11B and 30B, prepared with the similar surface treatment process as for Cloisite® 15A, have been depicted in Table 2.

### 3.2. Morphology of nanoclay inclusions by different mixing strategies

In order to compare the degree of intercalation and exfoliation, XRD patterns of 2, 4, and 6 wt.% of esterificated Cloisite® 11B-, 15A- and 30B-polyester nanocomposites prepared by stirring hotplate and five different mixing strategies were obtained. Curve (a) of Figure 5 shows the intensity data of the esterificated Cloisite® 15A-polyester nanocomposite prepared by stirring hotplate featuring a peak at 2.95° derived from the basal spacing in the range between 0° and 10°. On the other hand, the nanocomposites obtained by using mixing strategies I, II, and III shifted to lower peaks at 2.64° (curve (b)), 2.21° (curve (c)), and 2.15° (curve (d)), respectively. For the nanocomposites mixed with strategies IV and V, no peaks were observed (curves (e) and (f)). Therefore, the esterificated nanoclay interlayer distance calculated from Eq. (1) was 29.9 Å, 33.4 Å, 40.0 Å, and 41.1 Å for nanocomposites prepared by stirring hotplate and mixing strategies I, II, and III, respectively. Detecting no peaks in XRD graphs

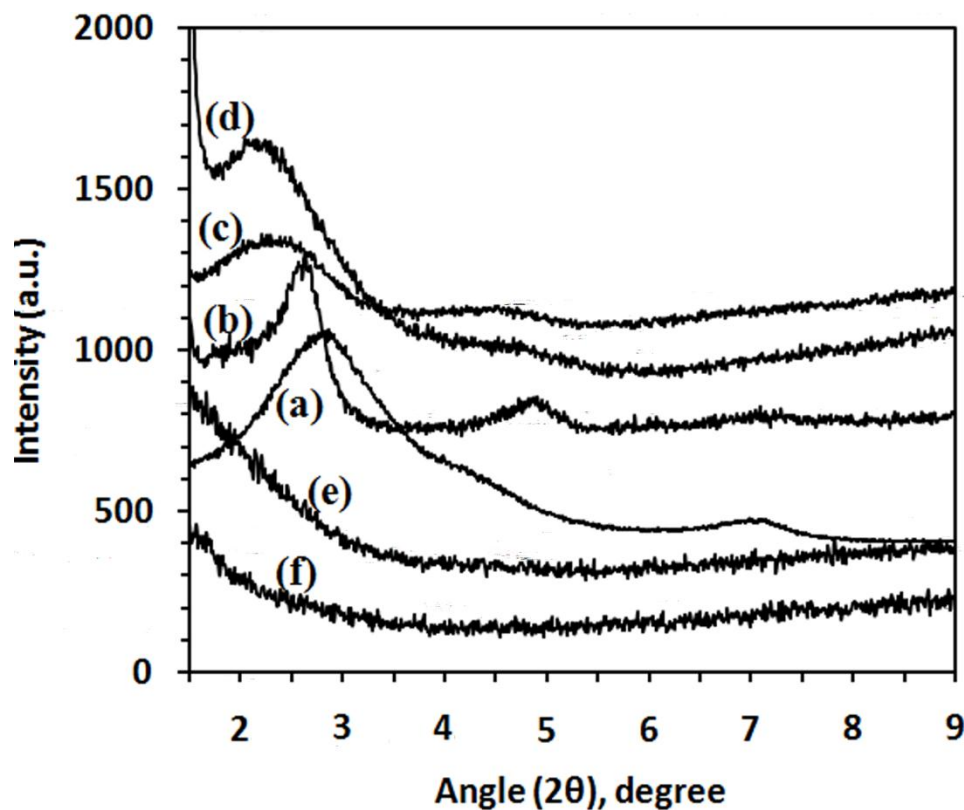


**Figure 5.** XRD patterns of 4 wt.% esterificated Cloisite® 15A-polyester samples prepared by (a) stirring hotplate (initial mixing), (b) strategy I, (c) strategy II, (d) strategy III, (e) strategy IV, and (f) strategy V.

for nanocomposites prepared according to mixing strategies IV and V confirms the formation of well intercalated and exfoliated nanoclay structure.

Table 2 depicts the interlayer  $d$ -spacing of different nanocomposite systems prepared according to the different surface treatments and five mixing strategies presented here. The numbers in the parentheses show the percentages of the  $d$ -spacing increases in comparison to those prepared by virgin Cloisites. For esterificated Cloisite® 11B- and Cloisite® 30B-polyester systems, although the interlayer  $d$ -spacing was increased up to 83% and 54% for nanocomposites prepared according to mixing strategy V, respectively; however none of our five mixing strategies led to a fully exfoliated structure since a peak was always observed in XRD results.

**Table 2.** Interlayer spacing-surface treatment and -mixing strategy correlations of different kinds of Cloisites in polyester matrix obtained from XRD measurements.

Cloisite®	Virgin	Precipitated in acetone	Alkyl chain grafted	Strategy I	Strategy II	Strategy III	Strategy IV	Strategy V
15A	24.6	25.2 (+2%)	29.9 (+22%)	33.4 (+36%)	40.0 (+63%)	41.1 (+67%)	---	---
11B	16.3	16.5 (+1%)	18.4 (+13%)	19.4 (+19%)	22.7 (+39%)	23.9 (+47%)	27.3 (+67%)	29.8 (+83%)
30B	16.7	17.0 (+2%)	18.5 (+11%)	21.3 (+28%)	22.5 (+35%)	23.6 (+41%)	25.2 (+51%)	25.7 (+54%)

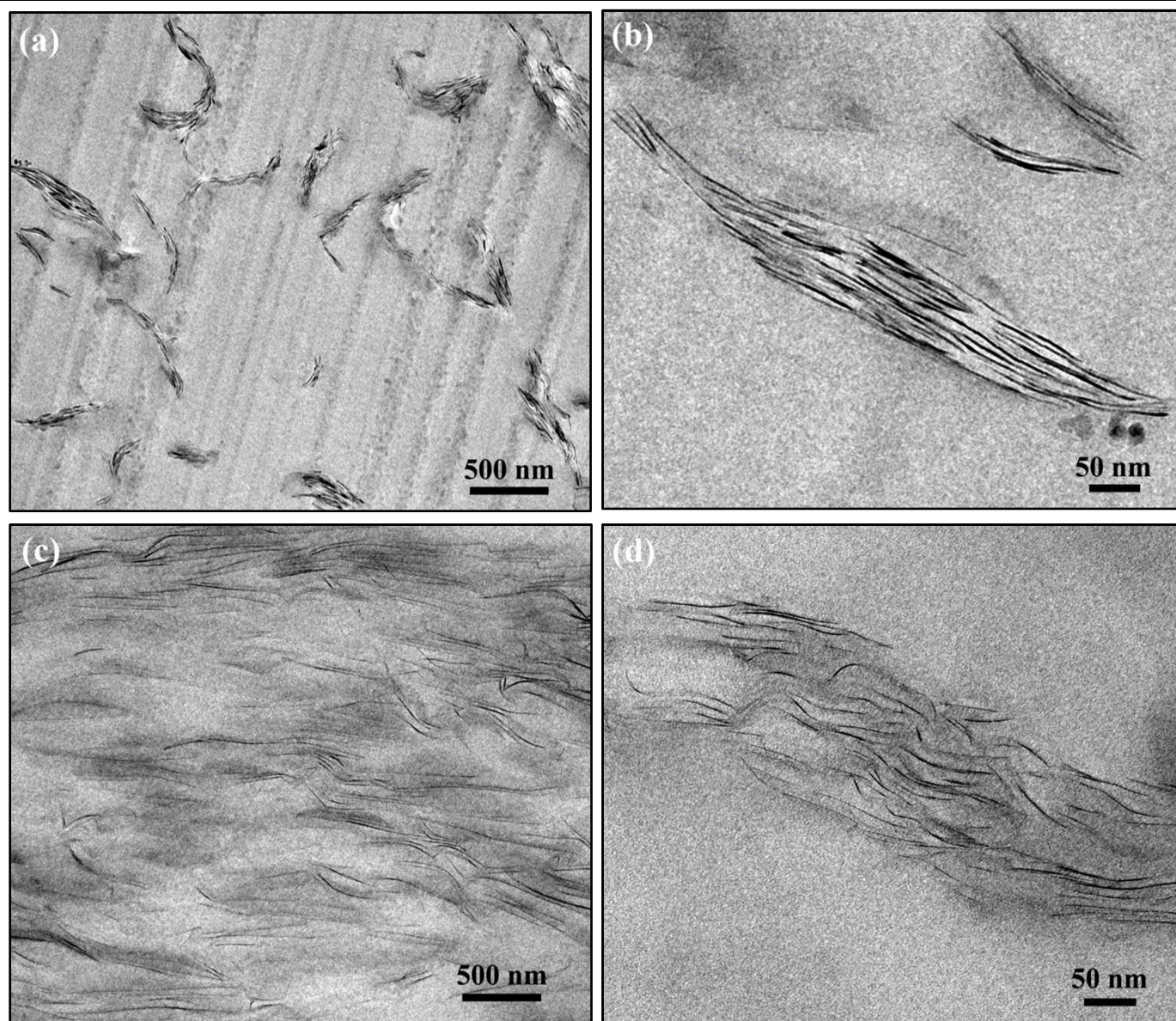


**Figure 6.** Low and high magnification TEM micrographs of 4 wt.% esterificated Cloisite® 15A-polyester samples prepared according to (a,b) mixing strategy II, and (c,d) mixing strategy IV.



1 Figure 6 shows the representative TEM images of 4 wt.% esterificated Cloisite® 15A-polyester  
2 samples prepared by mixing strategy II (a,b), and strategy IV (c,d). The bright region represents the  
3 matrix portion and the dark lines represent the clay nanolayers. The nanoclay aggregates in Figure 6a  
4  
5 matrix portion and the dark lines represent the clay nanolayers. The nanoclay aggregates in Figure 6a  
6  
7 show that the exfoliation of the clay nanolayers has not been uniformly reached throughout the  
8  
9 polyester. The corresponding higher magnification image (Figure 6b) shows the existence of  
10  
11 intercalated nanoclay structure inside the matrix. However, the esterificated nanoclay-polyester samples  
12  
13 prepared according to mixing strategy IV, show a more uniform dispersion (Figure 6c) of exfoliated  
14  
15 (Figure 6d) nanoclay which is in agreement with the results obtained from XRD patterns.  
16  
17  
18  
19

### 20 **3.3. Mechanical properties**

#### 21 **3.3.1 Tensile Modulus**

22  
23  
24  
25  
26  
27 The measured tensile modulus obtained from the initial slope of the stress-strain curve for virgin  
28  
29 polyester and polyester-based nanocomposites made with different mixing strategies and clay contents  
30  
31 are provided in Figure 7. The results have been averaged over five repetitions for each nanocomposite  
32  
33 system and the error bars were calculated based on the 95% confidence interval. The dashed horizontal  
34  
35 line corresponds to the virgin polyester data. The stiffness values obtained from the tensile tests revealed  
36  
37 a decrease of the tensile modulus due to the addition of nanoclay for the samples prepared using  
38  
39 strategies I, II, and III while an increase for those prepared by strategy IV and V. The nanocomposites  
40  
41 having 4 wt.% of esterificated nanoclay content showed a stiffness increase of 53%. The effect of  
42  
43 nanoclay content on stiffness of samples prepared by strategy IV was almost the same or even better  
44  
45 than those provided by strategy V and hence limited improvement was observed by increasing the  
46  
47 number of TRM passes over three.  
48  
49  
50  
51  
52

53  
54 Figure 8 shows the tensile modulus values of different polyester- esterificated nanoclay systems  
55  
56 obtained using mixing strategy IV. A significant enhancement in tensile modulus was observed for  
57  
58  
59  
60

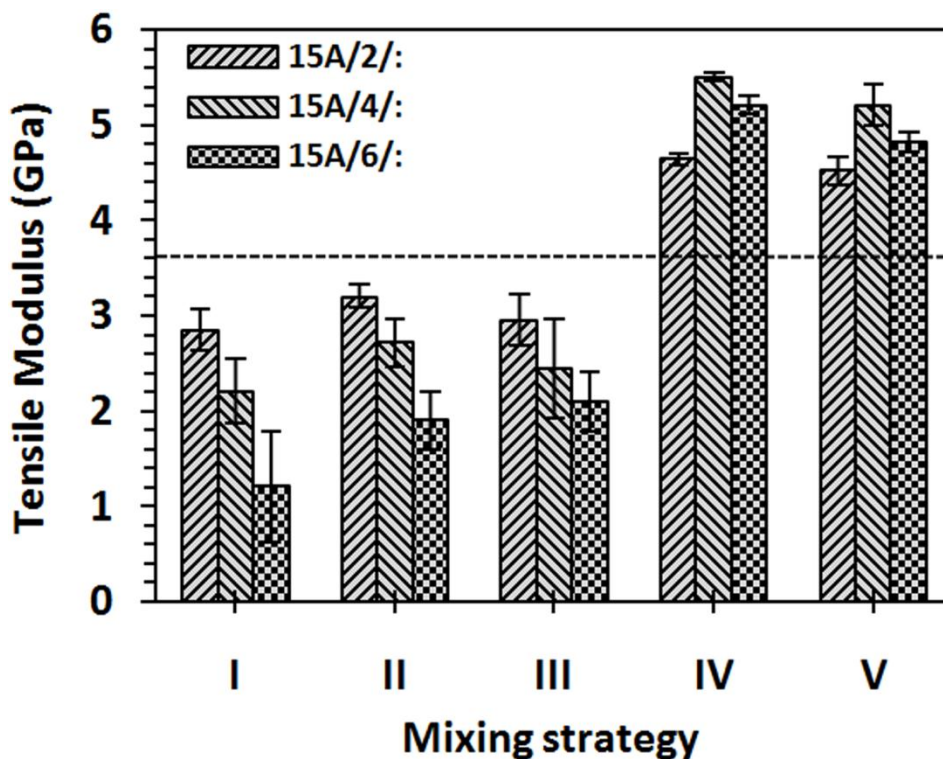


**Figure 7.** Experimental tensile modulus of polyester-based esterified Cloisite® 15A systems featuring different esterified nanoclay content and mixing strategy. Dotted horizontal line represents the baseline value of the virgin polyester.

esterified nanoclays having 2M2HT as surface modifier (Cloisite® 15A). The samples prepared with esterified Cloisite® 30B showed a decrease of  $\sim 42\%$  in modulus. This detrimental effect is probably due to the formation of phase separated nanoclay aggregates as confirmed from SEM and TEM images (not shown).

To demonstrate the effects of the degree of nanoclay dispersion in the improvement of the nanocomposite mechanical properties, the fracture surfaces of several polyester-esterified nanoclay systems were qualitatively analyzed. The roughness of the fracture surface has generally been associated to fracture properties and fracture energy release rates.<sup>52,53</sup> A smooth fracture surface is attributed to brittle failures and rougher fracture surfaces are attributed to tougher materials.<sup>53</sup> Figure 9a shows the

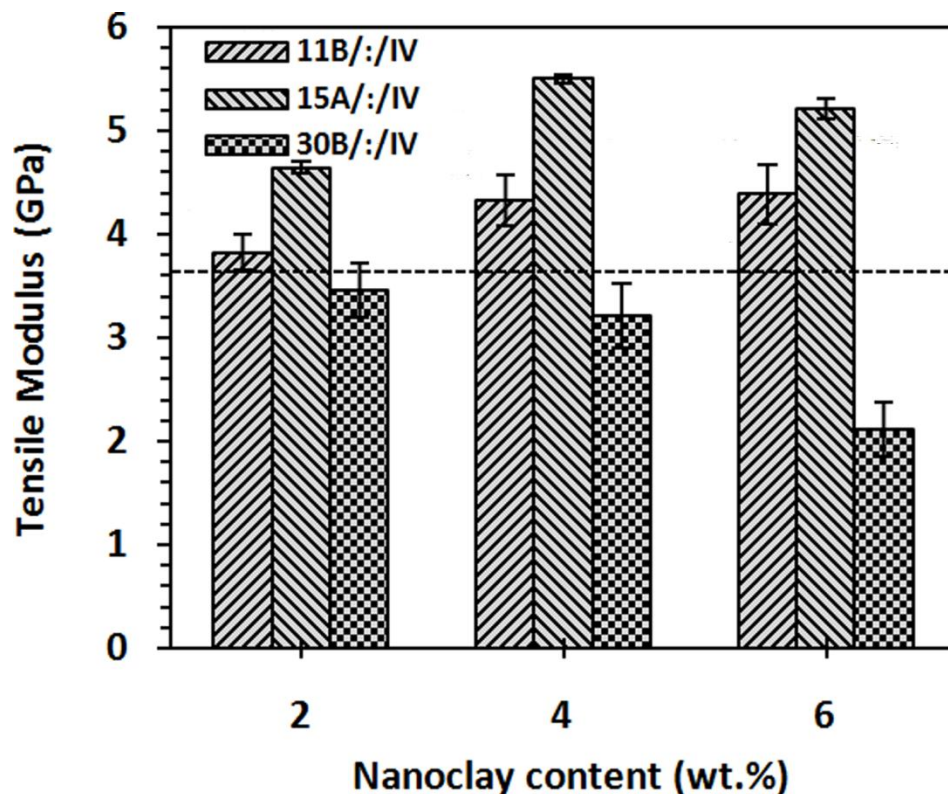


**Figure 8.** Experimental tensile modulus of polyester-based esterificated nanoclay systems having different nanoclay type and content. Dotted horizontal line represents the baseline value of the virgin polyester.

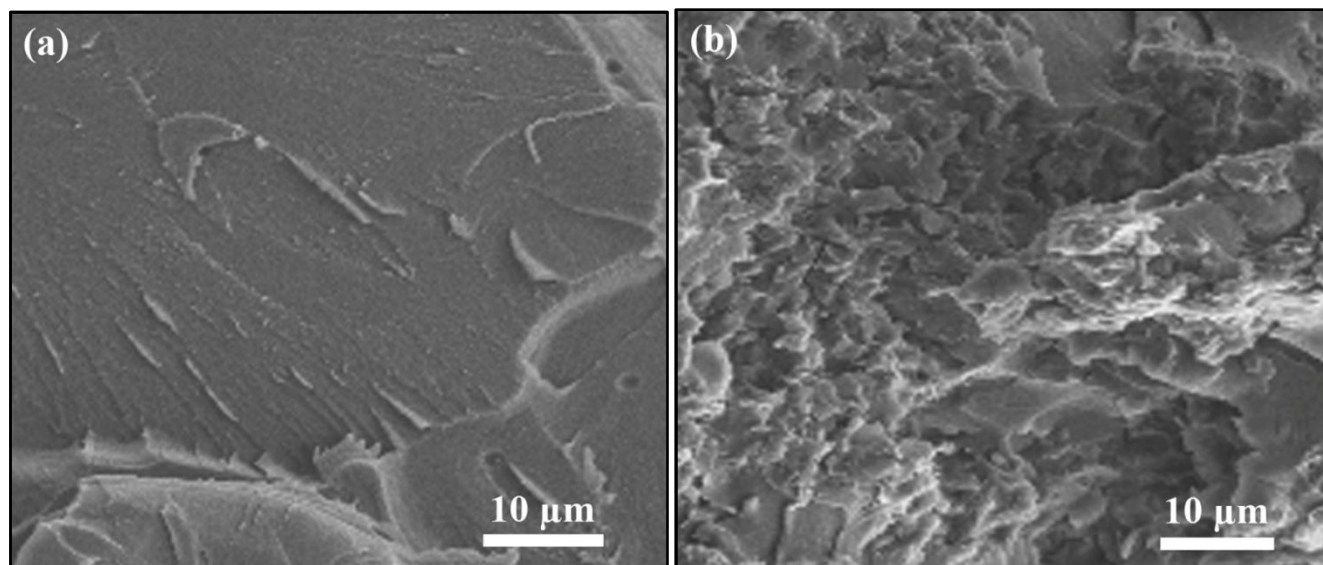


**Figure 9.** SEM images showing tensile fracture surface morphologies for the 4 wt.% esterificated Cloisite® 15A-polyester nanocomposites prepared according to (a) strategy II, and (b) strategy IV.

SEM images of the relatively smooth tensile fracture surface of the 4 wt.% esterificated Cloisite® 15A-polyester nanocomposites prepared according to strategy II. However, for the same system prepared according to strategy IV, significantly rougher fracture surfaces can be observed (Figure 9b), which proves the better dispersion of clay particles in the polyester matrix.

### 3.3.1.1 Modeling the effective stiffness

According to our XRD experiments, esterificated Cloisite® 15A particles prepared according to strategy IV seem to be well exfoliated in the polyester matrix. However, an indirect verification of the degree of exfoliation can be obtained using an effective medium theory. The idea is that no matter which theoretical model is chosen, it is necessary to make some assumptions about the degree of exfoliation. So the comparison between the experimentally determined Young's modulus with the theoretical predictions will indirectly give information about the degree of exfoliation. The Mori-Tanaka method<sup>54</sup> along with an orientation distribution function<sup>55</sup> was used to predict the effective stiffness of the polyester-based nanoclay nanocomposites. The effective Mori-Tanaka stiffness,  $\mathbf{k}^{(MT)}$ , of a two-phase material can be expressed as

$$\mathbf{k}^{(MT)} = \mathbf{k}_1 + f_2 \{ (\mathbf{k}_2 - \mathbf{k}_1) \mathbf{T} \} [f_2 \mathbf{I} + f_2 \{ \mathbf{T} \}]^{-1}, \quad (2)$$

where  $\mathbf{k}_1$  and  $\mathbf{k}_2$  are the fourth order stiffness tensors of the polyester matrix and the nanoclay particles, respectively. The volume fraction of the particles are denoted as  $f_2$ .  $\mathbf{I}$  is the fourth order identity tensor and  $\mathbf{T}$  is the Wu tensor<sup>56</sup> and is given as

$$\mathbf{T} = [\mathbf{I} + \mathbf{S} \mathbf{k}_1^{-1} (\mathbf{k}_2 - \mathbf{k}_1)]^{-1}, \quad (3)$$

where  $\mathbf{S}$  is the fourth order Eshelby tensor depending only on the aspect ratios of the particles and the properties of the matrix material.  $[\ ]^{-1}$  denotes the inverse and the curly brackets denotes averaging over

all possible orientations. Using the orientation function from<sup>54</sup>, the effective stiffness,  $\langle k_{ijkl} \rangle$ , of a two-phase material with particle orientation distribution function,  $g(\theta, \varphi, \beta)$ , is

$$\langle k_{ijkl} \rangle = \int_0^{2\pi} \int_0^{2\pi} \int_0^{2\pi} g(\theta, \varphi, \beta) a_{ip} a_{jq} a_{kr} a_{ls} k_{pqrs} \sin(\theta) d\theta d\varphi d\beta, \quad (4)$$

where  $g(\theta, \varphi, \beta)$ , is given as

$$g(\theta, \varphi, \beta) = \frac{\sin(\theta)^{2P-1} \cos(\theta)^{2Q-1}}{\int_{\theta_a}^{\theta_b} \sin(\theta)^{2P-1} \cos(\theta)^{2Q-1} d\theta}, \quad (5)$$

where  $\theta_a$  and  $\theta_b$  are the lower and upper limits of  $\theta$  being present in the distribution and  $0 \leq \theta_a$ ,  $\theta_b \leq \pi$  and  $P \geq \frac{1}{2}$ ,  $Q \geq \frac{1}{2}$  and finally  $a_{ij}$  is a function of the Euler angles  $(\theta, \varphi, \beta)$  defined in Appendix A.

The relevant measured modulus and Poisson's ratio of polyester RL7520 are  $E_{\text{RL7520}} = 3.6$  GPa and  $\nu_{\text{RL7520}} = 0.33$ . The similar data for the nanoclay particles are taken from.<sup>57,58</sup> In fact the nanoclay particles are transversely isotropic, but wang et al.,<sup>57,58</sup> compared the predicted effective stiffness when assuming isotropic and transversely isotropic particles, respectively and found the difference to be negligible. Thus, for simplicity the particles are considered to be isotropic with  $E_{\text{nanoclay}} = 107$  GPa and  $\nu_{\text{nanoclay}} = 0.30$ . The aspect ratios, i.e. length to thickness ratios, of the nanoclay particles given by the material supplier are in the range of 70-150, as it was also confirmed from TEM images, meaning that the nanoclay particles are of platelet shape. In the following an aspect ratio equal to 100 is chosen since the difference in effective stiffness of the two limits is less than 10% for the volume fractions considered in this work. The effective Young's modulus for polyester-based nanoclay nanocomposites with Mori-Tanaka random particle orientation ( $E^{MT}$ ) is compared to the experimental values ( $E^{EXP}$ ), the Voigt upper ( $E^U$ ) and Reuss lower ( $E^L$ ) bounds. The values obtained are shown in Table 3.

**Table 3.** Effective Young's modulus for polyester-based nanoclay nanocomposites with random particle orientation.  $E^L$ ,  $E^{EXP}$ ,  $E^{MT}$  and  $E^U$  are the Reuss lower bound, experimentally measured, Mori-Tanaka and Voigt upper bound values, respectively. The numbers in the parentheses show the percentages of the stiffness improvements in comparison to those of virgin polyester.

Effective stiffness	Nanoclay content (wt.%)		
	2	4	6
$E^L$ (GPa)	3.67 (+2%)	3.74 (+4%)	3.82 (+6%)
$E^{EXP}$ (GPa)	4.64 (+29%)	5.50 (+53%)	5.21 (+45%)
$E^{MT}$ (GPa)	5.04 (+40%)	6.44 (+79%)	7.85 (+118%)
$E^U$ (GPa)	5.65 (+57%)	7.74 (+115%)	9.79 (+172%)

As it can be seen from Table 3, the experimental values for 2 and 4 wt.% esterificated Cloisite® 15A are relatively close to that calculated with Mori-Tanaka model, which directly suggests that the nanoclay particles are relatively exfoliated, since that is the basic assumption in the modeling. The reason for the difference between the theoretical and the experimental results may be due to surface bonding effects which are not incorporated into the model in its present formulation. For higher volume fractions (e.g., 6 wt.%) the experimental values decrease and become much smaller than the theoretical predictions. This is most likely due to agglomeration of the particles and as a consequence the stiffness of the particles is not exploited to their full potential, thus not significantly increasing the effective stiffness of the composite. This has also been observed by<sup>59-61</sup> where the Young's modulus decreased for volume fractions above 2-3%.

### 3.3.2 Ultimate tensile strength

Figure 10 shows the ultimate tensile strength (UTS) results which are generally decreasing with the addition of esterificated nanoclay. However, adding 2 and 4 wt.% of esterificated Cloisite® 15A leads

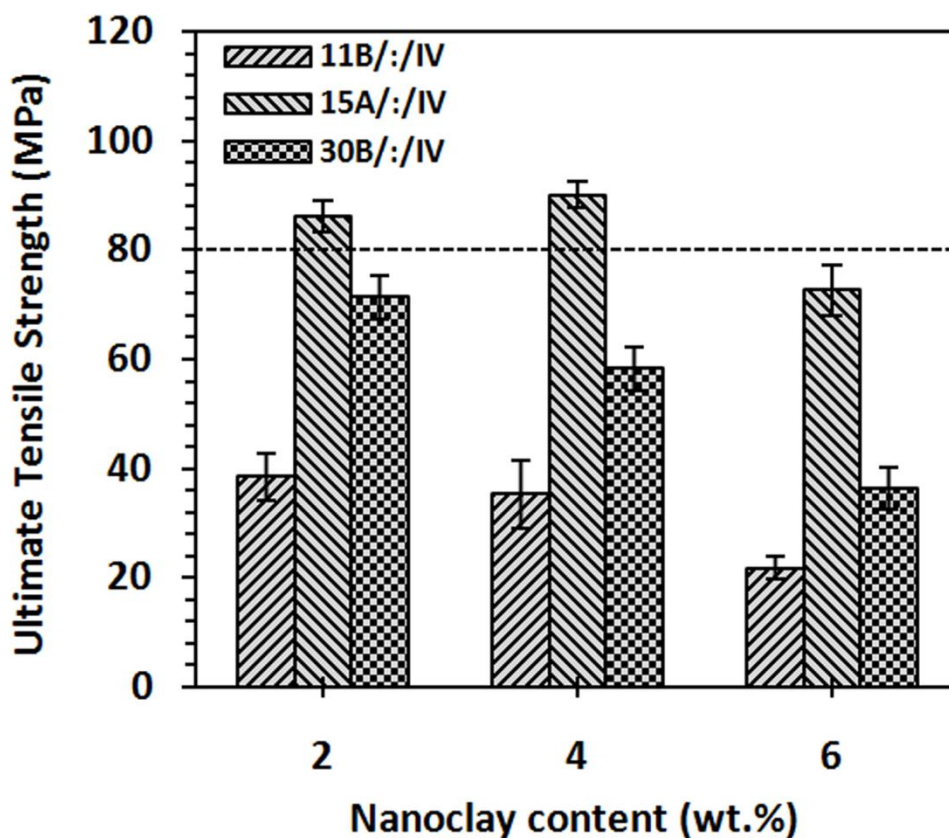


**Figure 10.** Experimental UTS values of polyester-based nanoclay systems having different esterificated nanoclay type and content. Dotted horizontal line represents the baseline value of the virgin polyester.

to 9% and 13% improvement in UTS, respectively. For 15A/6/IV system, the UTS reduces by 25% in comparison with 15A/4/IV which is believed to be attributed to the stiffening effect of adding further nanoclay leading to more brittle nanocomposites systems.

### 3.3.3 Elongation at break

The elongation at break is reported in Figure 11. The ductility of the nanocomposites is generally reduced with increasing the nanoclay content. Significant differences in failure elongations were observed for 30B/IV systems (: is a notation representing all the nanoclay contents tested) in comparison with those of 11B/IV and 15A/IV. For 15A/IV systems, ~ 31% more deterioration in failure strains was observed in comparison to that of 30B/IV which can be attributed to the higher aspect ratio of Cloisite® 15A after mixing, measured from TEM images (not shown).

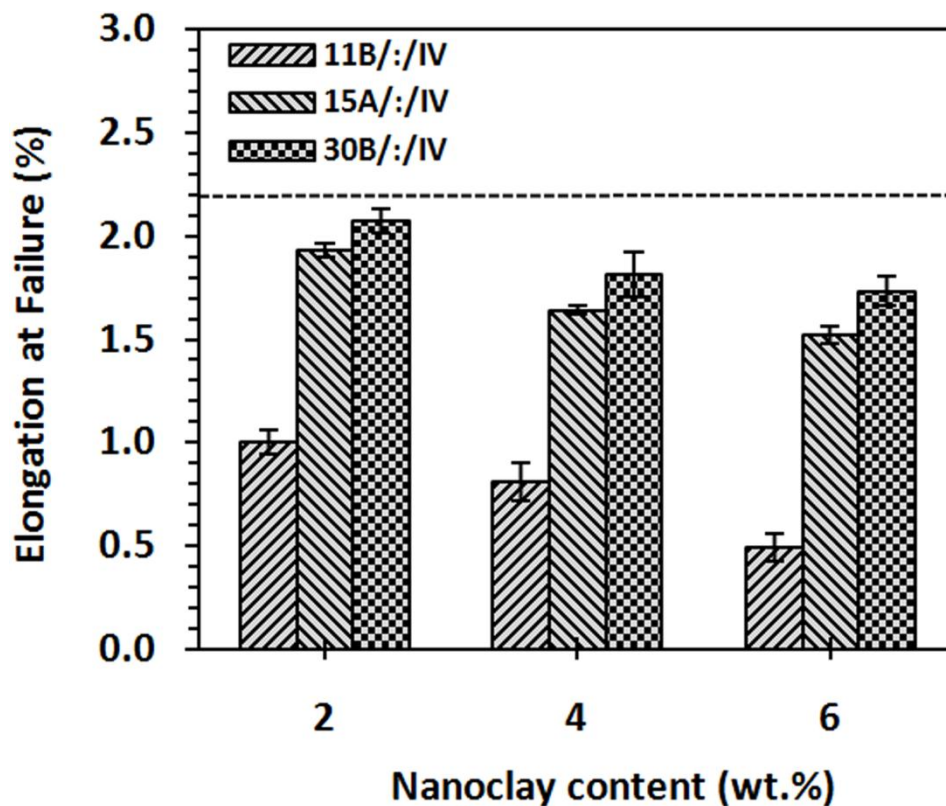


**Figure 11.** Experimental tensile test elongations at break of polyester-based esterificated nanoclay systems having different nanoclay type and content. Dotted horizontal line represents the baseline value of the virgin polyester.

### 3.4. Thermal properties

The CTE above and below  $T_g$  are provided in Figure 12 for the specimens prepared according to strategy IV (i.e., batch numbers 4, 9, 14, 19, 24, 29, 34, 39 and 44 in Table 1). The variation of  $T_g$  for nanocomposites with varying nanoclay type and content is also shown in Figure 13. For structural applications the CTE above  $T_g$  is not of much importance as by this point the load carrying capacity is considerably reduced. As a result, only discussions on CTE results below  $T_g$  are presented. Nonetheless, CTE values below and above  $T_g$  follow similar trends and thus the observations noted here are also valid for CTE values above  $T_g$ .



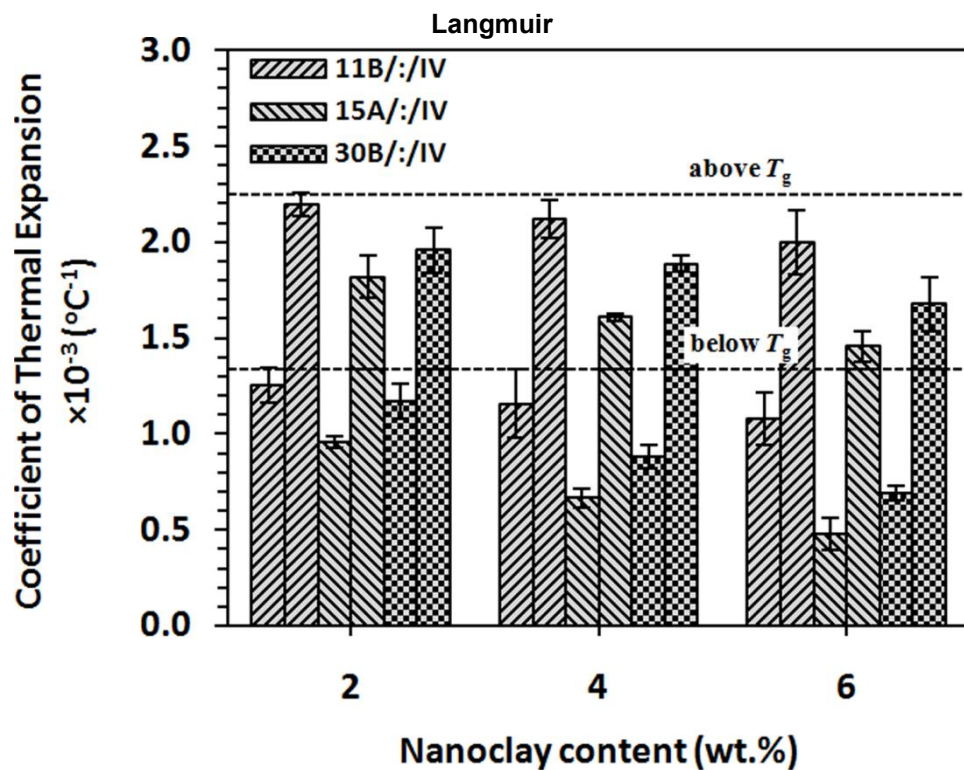


**Figure 12.** Variation of CTE below (left column) and above (right column)  $T_g$  of polyester-based nanoclay systems having different esterificated nanoclay type and content. Dotted horizontal line represents the baseline values of CTE below and above  $T_g$  of the virgin

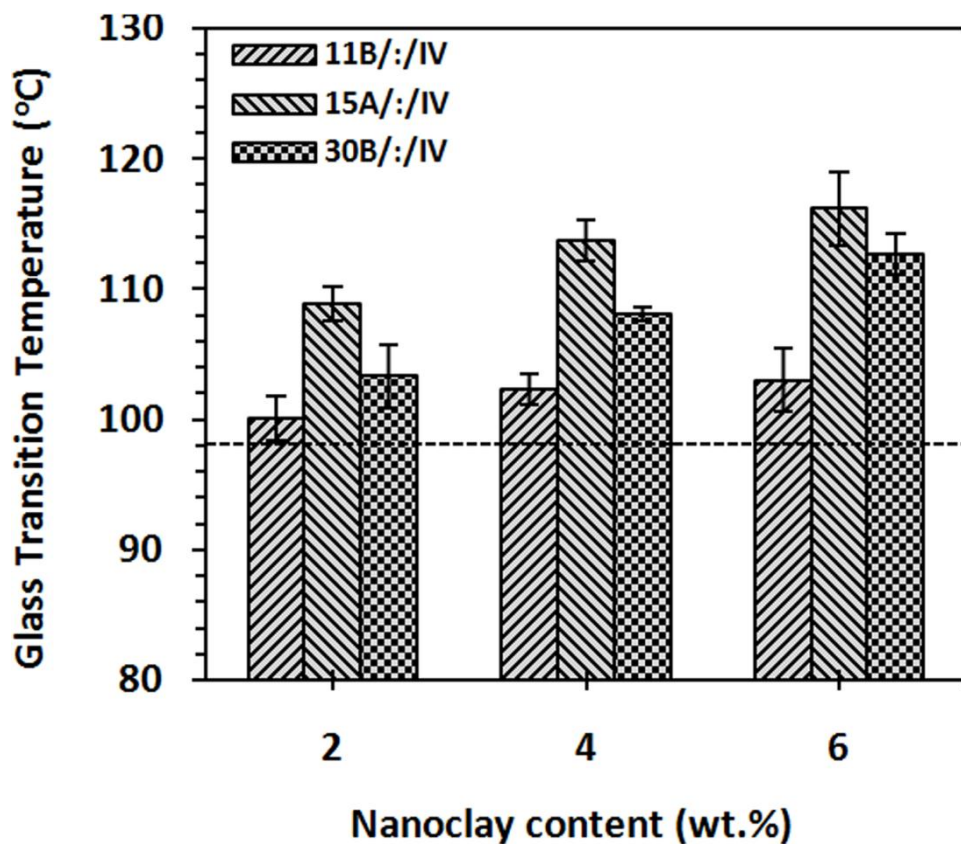


**Figure 13.** Variation of glass transition temperature ( $T_g$ ) of polyester-based nanoclay systems having different esterificated nanoclay type and content. Dotted horizontal line represents the baseline value of the virgin polyester.

The addition of nanoclay generally decreased the CTE of the polyester-based nanocomposite compared to that of plain resin. In general, the thermal properties (CTE and  $T_g$ ) due to nanoclay addition were better than the corresponding neat resin values, specially for 15A/4/IV and 15A/6/IV systems with an improvement of up to 16 °C and 18 °C in  $T_g$ , respectively.

### 3.5. Moisture absorption

The moisture diffusivity coefficient  $D$ ,<sup>39</sup> was used as the parameter to assess the effect of nanoclay type and content and was computed from the initial slope of the moisture gain  $M_t/M_\infty$  versus time ( $\sqrt{t}/d$ ) based on Fick's law:<sup>62</sup>

$$D = \frac{\pi}{16} \left( \frac{M_t/M_\infty}{\sqrt{t}/d} \right)^2, \quad (6)$$

where  $M_t$  is the mass gain at any time  $t$ ,  $M_\infty$  is the maximum mass gain at equilibrium/steady state, and  $d$  is the thickness of the specimen.

The diffusivity coefficient of all polyester-based nanocomposites obtained using the mixing strategy IV has been summarized in Figure 14. As for the thermal properties, esterificated nanoclay addition increased the barrier properties (i.e., reduced diffusivity). Overall, noticeable decrease in diffusivity of up to 370% was observed in 15A/4/IV and 15A/6/IV systems.

A diffusion model of intercalated nanoclays inside a polymer matrix was previously developed by Liu et al.,<sup>63</sup> by using a Fickian numerical model<sup>39</sup> and assuming that the nanoclays have been randomly oriented and uniformly dispersed inside the polymer as;

$$D^* = \frac{1}{\left(1 + \frac{2\zeta f_c}{3\pi n}\right)^2}, \quad (7)$$

where  $D^*$  is diffusivity ratio, i.e. diffusivity of nanocomposite to that of virgin polyester;  $\zeta$ ,  $f_c$  are the

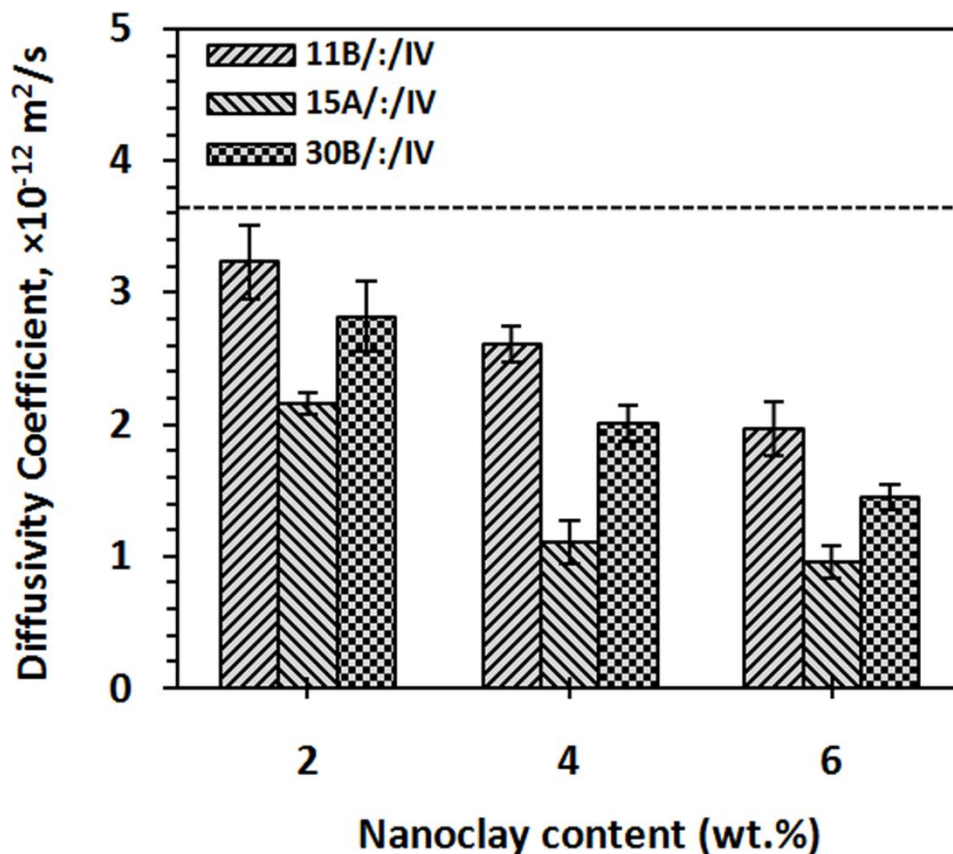


**Figure 14.** Experimental diffusivity coefficients of polyester-based nanoclay systems having different esterificated nanoclay type and content. Dotted horizontal line represents the baseline value of the virgin polyester.

aspect ratio and volume fraction of the nanoclays inside the matrix, respectively.  $n$  is the number of clay platelets in each agglomerate. Based on equation (7),  $D^*$  in nanoclay nanocomposites decreases with increasing the clay loading and the aspect ratio, while an increase should be expected when clay agglomerates inside the polymer matrix include higher number of platelets.

Curves based on the Fickian diffusivity model for intercalated nanocomposites have been plotted in Figure 15. As it can be seen, the experimental diffusivity values for esterificated Cloisite® 15A polyester-based nanocomposites prepared according to mixing strategy IV fall between the model prediction curves for nanoclays having either 1 or 2 clay platelets in agglomerates which confirms the fully exfoliated nanoclay structure as it was also observed from TEM images (Figure 6c-d). The

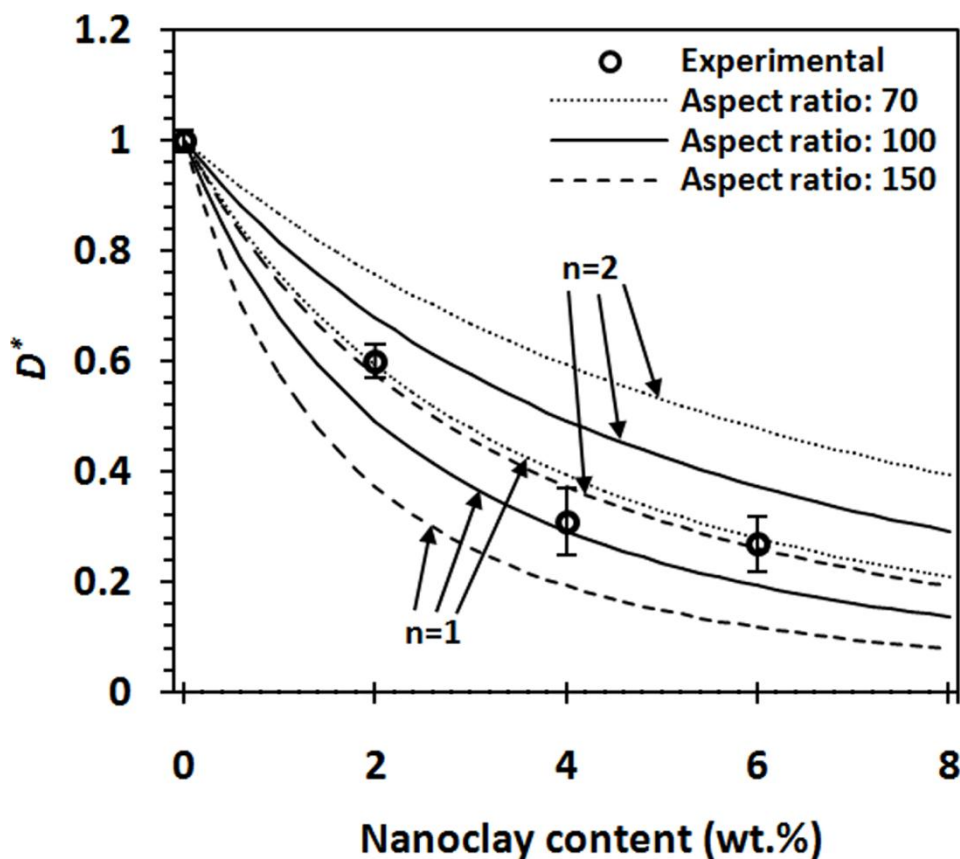


**Figure 15.** Diffusivity ratio ( $D^*$ ) obtained by mixing strategy IV for esterificated Cloisite® 15A-polyester systems versus clay content, at 50 °C.

comparison among the experimental diffusivity measurements and those of theoretical estimations suggests a value between 100-150 for the aspect ratio of the nanoclays after performing several times three-roll mixing and ultrasonication. This is in the same aspect ratio range of nanoclays before mixing with polyester matrix suggesting the fact that during the mixing process no breakage in nanoclay structure occurred.

#### 4. General Discussion

The experimental characterization of our different polyester-based nanoclay nanocomposites revealed that the combination of nanoclay type, surface treatment, content, and mixing strategies resulted in producing materials having superior, similar, or even inferior mechanical, thermal, and barrier properties in comparison with those of the virgin polyester matrix.

#### 4.1. Surface treatment analysis

1  
2  
3  
4 Clay platelets modified with ammonium ions carrying hydroxyl groups were surface reacted with  
5  
6 long chain fatty acids in order to achieve enhancement in their basal plane spacing so as to achieve their  
7  
8 shear induced exfoliation in the polymer matrices. The extent of surface reaction enhanced with  
9  
10 increasing the amount of excess acid used for the reaction which subsequently increased the basal plane  
11  
12 spacing. The XRD analysis showed an increase of the  $d$ -spacing of the Cloisite® 15A from 24.6 Å to  
13  
14 25.2 Å when suspended in acetone and to 29.9 Å for the alkyl chain grafted clays indicating a slightly  
15  
16 exfoliated structure. The initial higher basal plane spacing of the surface treated clay platelets led to  
17  
18 better swelling of the montmorillonite resulting in the enhancement of the basal plane spacing. FTIR  
19  
20 diagram revealed the ionically bonding of high density brushes to the clay surface when the initial  
21  
22 modification was optimal to generate higher extents of surface reaction.  
23  
24  
25  
26  
27

#### 4.2. Physical behavior characterization

28  
29  
30  
31 The maximum stiffness for all nanocomposite systems were obtained when combined TRM and US  
32  
33 were used (strategies IV and V). Strategies I, II, and III, generally led to a decrease in modulus up to  
34  
35 39% for 15A/4/I while an increase of 53% for 15A/4/IV. Moreover, the tensile modulus did not even  
36  
37 follow similar trends for different types and contents of esterificated nanoclay. For example, a  
38  
39 continuous increase in modulus was observed for 11B:/IV systems by increasing the esterificated  
40  
41 nanoclay content, while an inverse behavior for 30B:/IV systems. On the other hand for 15A:/IV, the  
42  
43 maximum modulus was obtained when 4 wt.% esterificated nanoclay was added.  
44  
45  
46  
47  
48

49 The tensile tests also revealed an overall reduction in ductility and strength due to the addition of  
50  
51 nanoclay. The increase in strength up to 13% was only observed when 2 and 4 wt.% esterificated  
52  
53 Cloisite® 15A was mixed according to strategy IV. The strength of 15A:/IV systems decreased with an  
54  
55 increase in the nanoclay content over 4 wt.% (i.e., 8% strength loss for 15A/6/IV system). A reduction  
56  
57 of 55% in strength for 11B/4/IV in comparison to the gain of 13% for 15A/4/IV is attributed to the type  
58  
59  
60

1 of the surface modifiers used, suggesting esterificated Cloisite® 15A as a more suitable reinforcement  
2 for this type of the polyester-based nanocomposites. The reduced UTS values in 11B/IV and 30B/IV  
3 systems are believed to be due to the weaker nanoclay-polyester interface and consequently the creation  
4 of the nanoclay aggregates in the polyester matrix, which promotes microcrack formation and leads to  
5 the formation of nanocomposites having lower tensile strength and ductility. While there is no general  
6 consensus on this point of view, computational studies by Haq et al.<sup>64</sup> have shown evidence to this  
7 mechanism.  
8  
9

10 The CTE and the moisture diffusivity also showed a noticeable improvement of up to 270% and  
11 370% for 15A/6/IV system which is due to choosing the right type and amount of esterificated nanoclay  
12 and mixing strategy. The addition of higher contents of esterificated nanoclay into polyester system  
13 generally resulted in nanocomposites with inferior thermal and barrier properties. The improvements in  
14 barrier properties could be explained by considering the physical aspects of the diffusion. During the  
15 diffusion process, the clay platelets act as impervious barriers to permeant molecules, thereby forcing a  
16 tortuous diffusion path that improves moisture barrier property. The use of a similar analogy for the  
17 CTE suggests that the expansion of the polymer network due to heat is higher than the restraining action  
18 provided by the nanoclay, which results in the nanoclay platelets moving along with the polymer under  
19 temperature expansion and consequently a decrease in CTE values which is considered as improvement  
20 in the thermal properties.  
21  
22  
23  
24  
25  
26  
27  
28  
29  
30  
31  
32  
33  
34  
35  
36  
37  
38  
39  
40  
41  
42

43 Although our experimental results showed that improvements in mechanical, thermal and barrier  
44 properties are possible for polyester-based esterificated nanoclay nanocomposites, the material  
45 composition that yields the best gain for a given property is different. Thus, when multiple properties  
46 are of interest, optimized material compositions that balance the improvements and detriments of the  
47 polyester system are needed.  
48  
49  
50  
51  
52  
53  
54  
55  
56  
57  
58  
59  
60

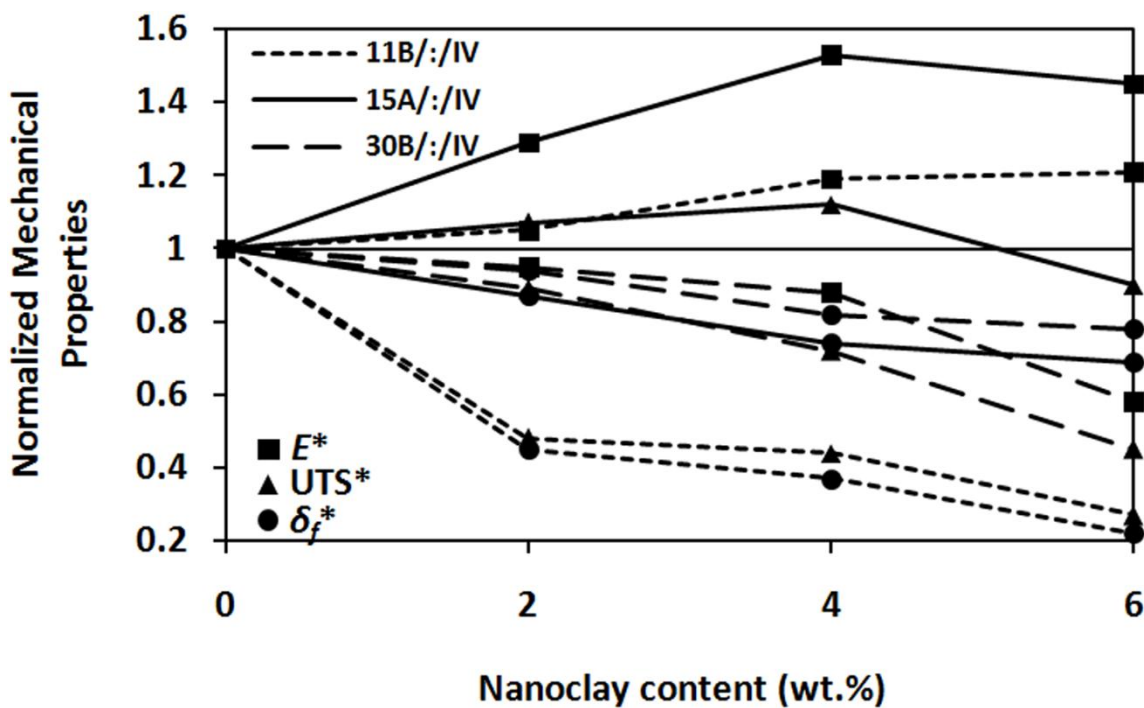


**Figure 16.** Normalized mechanical properties and identification of optimized material constituents.

Notation \* shows the normalized property of the polyester-based nanocomposite relative to that of the virgin polyester.

#### 4.3. Performance limits and optimized material design

Detailed experimental characterization of polyester-based esterified nanoclay nanocomposites with up to 6 wt.% of different types of esterified nanoclay allows obtaining performance limits of the resulting properties. Optimal material combinations that result in a balance of multiple properties, along with ease in processing are thus identified. According to the results obtained in this paper, esterified nanoclay reinforcement of more than 4 wt.% has generally little or sometimes negative effect on the mechanical properties of the nanocomposites. However, the thermal and barrier properties are continuously improving with the addition of esterified nanoclay up to 6 wt.%, ranking the samples having 6 wt.% of esterified nanoclay (:/6/IV) as the optimal designs.

Figures 16 and 17 show a comparison of mechanical properties such as stiffness (modulus,  $E$ ),

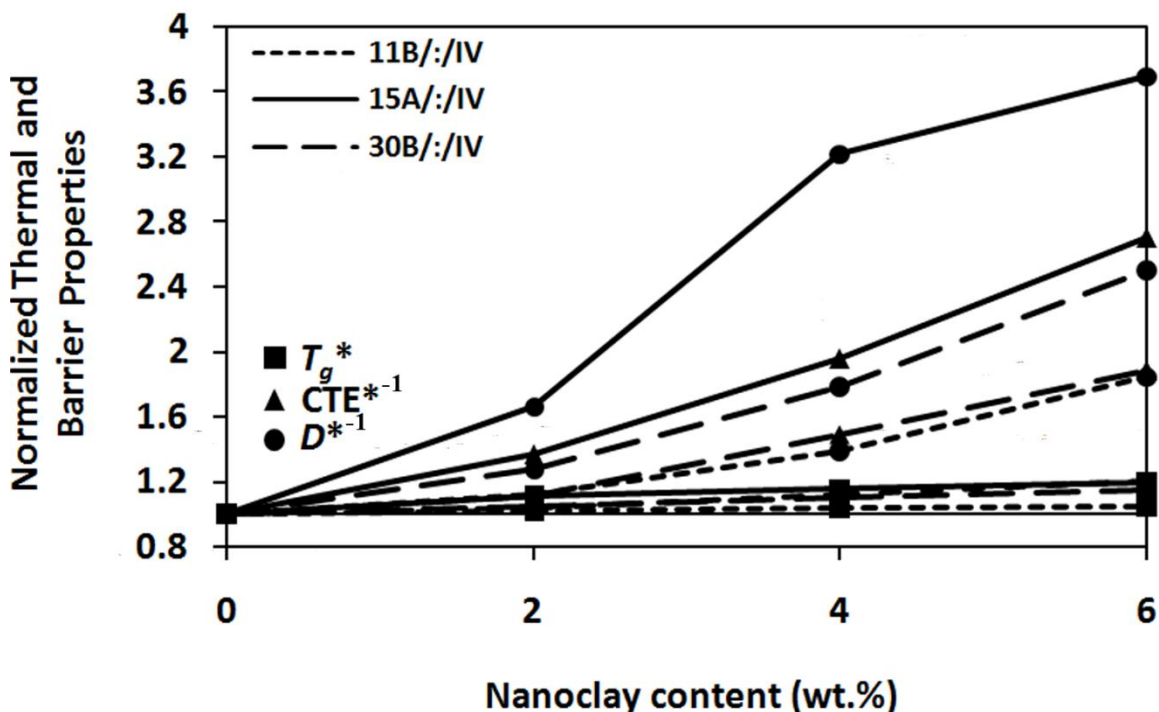


**Figure 17.** Normalized thermal and barrier properties and identification of optimized material

constituents. Notation \* shows the normalized property of the polyester-based nanocomposite relative to that of the virgin polyester.

strength (UTS) and ductility (elongation at failure,  $\delta_f$ ), and thermal and barrier properties namely thermal stability (glass transition temperature,  $T_g$ ; coefficient of thermal expansion, CTE) and diffusivity (diffusivity coefficient,  $D$ ). Notation \* shows the normalized property of the polyester-based nanocomposite relative to that of the virgin polyester for mechanical properties and glass transition temperature. For the coefficient of thermal expansion and diffusivity,  $CTE^*$  and  $D^*$  are inversed resulting in values greater than unity to show improvements in all properties. The general trend for the values of stiffness and ductility confirms that the addition of esterificated nanoclay improves stiffness for 15A/IV and 11B/IV while reducing its ductility; however, in case of 30B/IV both stiffness and ductility decrease. It should be noted that the area of interest in Figures 16 and 17 is subjective and can be determined based on the target properties and the material application. If properties strictly better than the baseline polyester are desired, constituent concentrations that satisfy such requirements can thus be selected. Generally, when multiple opposing parameters are considered, material constituents



1 that reveal good balance without significant compromise on other properties are sought. Overall,  
2 15A/4/IV and 15A/6/IV systems were identified as optimized material compositions as they show  
3 promise in their processing ease and balanced properties.  
4  
5  
6  
7

## 8 **5. Conclusion**

9  
10  
11 Results from this study indicate that various nanoclay types, surface treatments and contents can be  
12 mixed with polyesters in different ways to produce polyester-based nanocomposites with desired  
13 mechanical, thermal and barrier properties. This study aimed at finding an optimum mixing strategy of  
14 the proposed surface reacted nanoclays with polyesters based on the three-roll mill mixing, the  
15 ultrasonication, or a combination of both. It was shown that depending on the nanoclay type, surface  
16 treatment and mixing strategy, the addition of nanoclay into nanocomposites may improve mechanical  
17 (stiffness and strength) parameters and transient (thermal and moisture diffusion) properties; however it  
18 generally adds to their brittleness which could not be favorable. The efficiency of the nanoclay addition  
19 depends on many factors including the chemistry of the surface modifiers and their treatments, the  
20 mixing strategy selected, the nanoclay content and their level of dispersion. An extended experimental  
21 test matrix (up to 6 wt.% of three different kind of nanoclay along with five mixing strategies) with  
22 detailed characterization of mechanical and transient properties allowed obtaining the performance  
23 limits of these nanocomposite materials. Including ease of processing along with the resulting balanced  
24 or enhanced properties, polyester-based nanocomposites reinforced with 4 and 6 wt.% esterificated  
25 Cloisite® 15A were identified as optimal designs.  
26  
27  
28  
29  
30  
31  
32  
33  
34  
35  
36  
37  
38  
39  
40  
41  
42  
43  
44  
45  
46  
47

48 XRD analyses and TEM observations suggested the formation of exfoliated structures in  
49 15A/2,4/IV systems. The Mori-Tanaka method was used to predict the effective stiffness of the  
50 15A/2,4/IV nanocomposite systems which were in close agreement with those of the experimental  
51 values. Water diffusion behavior of polyester-nanoclay systems was found to follow very closely the  
52 Fickian behavior at 50 °C. As esterificated nanoclay was mixed into polyester according to strategy IV,  
53  
54  
55  
56  
57  
58  
59  
60

1 diffusivity was improved about 370% at 6 wt.% clay loading. The model for diffusivity for 15A/2,4/IV  
2 predicted the platelets to contain either 1 or 2 sheets of clay (i.e., exfoliated structure) and this agreed  
3 well with TEM observations.  
4  
5  
6  
7

8 For 15A/4/IV system, the tensile modulus and strength were increased by 53% and 13% compared  
9 to those of virgin polyester. The maximum improvement in CTE and moisture diffusivity of 270% and  
10 370% were obtained for 15A/6/IV system, respectively. Overall, the balanced behavior of the  
11 showcased polyester-based esterificated nanoclay nanocomposites shows promise for high-performance  
12 materials in automotive, transportation and packaging industry.  
13  
14  
15  
16  
17  
18  
19

## 20 **Acknowledgement**

21 The authors acknowledge the financial support from NSERC (the Natural Sciences and Engineering  
22 Research Council of Canada). They also acknowledge the technical support of NRC-IMI (the National  
23 Research Council-Industrial Materials Institute) with TEM and SEM imaging and members of CREPEC  
24 (Centre de Recherche En Plasturgie Et Composites), Dr. Nadir Kchit for his technical assistance in  
25 performing some of the mechanical tests and Amine El Mourid for developing the mechanical models.  
26  
27  
28  
29  
30  
31  
32  
33  
34  
35  
36  
37  
38  
39  
40  
41  
42  
43  
44  
45  
46  
47  
48  
49  
50  
51  
52  
53  
54  
55  
56  
57  
58  
59  
60

**Appendix A:  $a_{ij}$  coefficients as a function of the Euler angles**

1  
2  
3  
4  
5  
6  
7  
8  
9  
10  
11  
12  
13  
14  
15  $a_{11} = \cos(\theta)\cos(\varphi)\cos(\beta) - \sin(\varphi)\sin(\beta),$   
16

17  
18  $a_{12} = -\cos(\theta)\cos(\varphi)\sin(\beta) - \sin(\varphi)\cos(\beta),$   
19

20  
21  $a_{13} = \sin(\theta)\cos(\varphi),$   
22

23  
24  $a_{21} = \cos(\theta)\sin(\varphi)\cos(\beta) + \cos(\varphi)\sin(\beta),$   
25

26  
27  $a_{22} = \cos(\theta)\sin(\varphi)\sin(\beta) + \cos(\varphi)\cos(\beta),$   
28

29  
30  $a_{23} = \sin(\theta)\sin(\varphi),$   
31

32  
33  $a_{31} = -\sin(\theta)\cos(\beta),$   
34

35  
36  $a_{32} = \sin(\theta)\sin(\beta),$   
37

38  
39  $a_{33} = \cos(\theta).$   
40  
41  
42  
43  
44  
45  
46  
47  
48  
49  
50  
51  
52  
53  
54  
55  
56  
57  
58  
59  
60

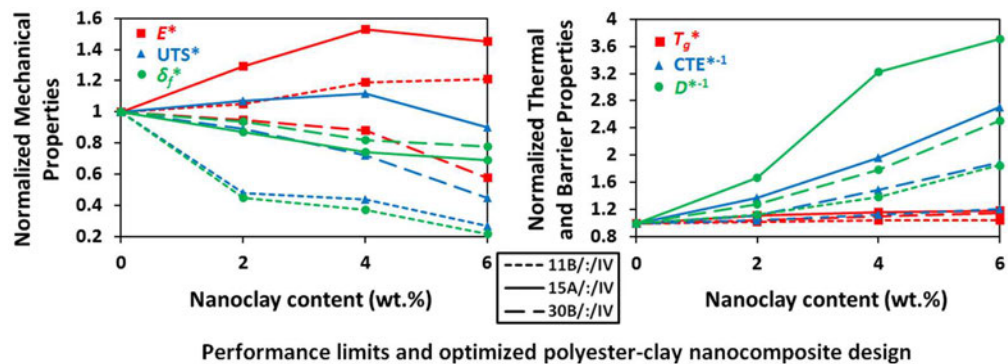
## References

- 1
- 2
- 3 (1) Pinnavaia, T. J. Intercalated clay catalysts. *Science* **1983**, *220* (4595), 365-371.
- 4 (2) Fukushima, Y.; Okada, A.; Kawasumi, M.; Kurauchi, T.; Kamigaito, O. Swelling behaviour of
- 5 montmorillonite by poly-6-amide. *Clay Minerals* **1988**, *23* (1), 27-34.
- 6 (3) Bailey, S. W. Reviews in mineralogy. *Mineralogical Society of America* **1984**, Blacksburg.
- 7 (4) Bailey, S. W. Crystal structure of clay minerals and their X-ray identification. *Mineralogical*
- 8 *Society* **1980**, London.
- 9 (5) Theng, B. K. G. The chemistry of clay-organic reactions. *Adam Hilger* **1974**, London.
- 10 (6) Lagaly, G.; Beneke, K. Intercalation and exchange reactions of clay minerals and non-clay layer
- 11 compounds. *Colloid Polym. Sci.* **1991**, *269* (12), 1198-1211.
- 12 (7) Osman, M. A.; Mittal, V.; Suter, U. W. Poly(propylene)-layered silicate nanocomposites: gas
- 13 permeation properties and clay exfoliation. *Macromol. Chem. Phys.* **2007**, *208* (1), 68-75.
- 14 (8) Osman, M. A.; Rupp, J. E. P.; Suter, U. W. Gas permeation properties of polyethylene-layered
- 15 silicate nanocomposites. *J. Mater. Chem.* **2005**, *15* (1), 1298-1304.
- 16 (9) Kawasumi, M.; Hasegawa, N.; Kato, M.; Usuki, A.; Okada, A. Preparation and mechanical
- 17 properties of polypropylene-clay hybrids. *Macromolecules* **1997**, *30* (20), 6333-6338.
- 18 (10) Oya, A.; Kurokawa, Y.; Yasuda, H. Factors controlling mechanical properties of clay
- 19 mineral/polypropylene nanocomposites. *J. Mater. Sci.* **2000**, *35* (5), 1045-1050.
- 20 (11) Xu, W.; Liang, G.; Wang, W.; Tang, S.; He, P.; Pan, W. P. PP-PP-g-MAH-Org-MMT
- 21 nanocomposites. I. Intercalation behavior and microstructure. *J. Appl. Polym. Sci.* **2003**, *88* (14),
- 22 3225- 3231.
- 23 (12) Persson, H. H. J.; Caseri, W. R.; Suter, U. W. Versatile method for chemical reactions with
- 24 selfassembled monolayers of alkanethiols on gold. *Langmuir* **2001**, *17* (12), 3643-3650.
- 25 (13) Guiomar, A. J.; Guthrie, J. T.; Evans, S. D. Use of mixed self-assembled monolayers in a study
- 26 of the effect of the microenvironment on immobilized glucose oxidase. *Langmuir* **1999**, *15* (4),
- 27 1198-1207.
- 28 (14) Lofas, S.; Johnsson, B. A novel hydrogel matrix on gold surfaces in surface plasmon
- 29 resonance sensors for fast and efficient covalent immobilization of ligands. *J. Chem. Soc. Chem.*
- 30 *Commun.* **1990**, *21* (1), 1526-1528.
- 31 (15) Wilner, I.; Riklin, A.; Shoham, B.; Rivenson, D.; Katz, E. Development of novel biosensor
- 32 enzyme electrodes: Glucose oxidase multilayer arrays immobilized onto self-assembled
- 33 monolayers on electrodes. *Adv. Mater.* **1993**, *5* (12), 912-915.
- 34 (16) Pan, S.; Castner, D. G.; Ratner, B. D. Multitechnique surface characterization of derivatization
- 35 efficiencies for hydroxyl-terminated self-assembled monolayers. *Langmuir* **1998**, *14* (13), 3545-
- 36 3550.
- 37 (17) Yan, L.; Huck, W. T. S.; Zhao, X. M.; Whitesides, G. M. Patterning thin films of
- 38 poly(ethyleneimine) on a reactive SAM using microcontact printing. *Langmuir* **1999**, *15* (4),
- 39 1208-1214.
- 40 (18) Evans, S. D.; Sharma, R.; Ulman, A. Contact angle stability: Reorganization of monolayer
- 41 surfaces?. *Langmuir* **1991**, *7* (1), 156-161.
- 42 (19) Tyan, H. L.; Liu, Y. C.; Wei, K. H. Thermally and mechanically enhanced clay/polyimide
- 43 nanocomposites via reactive organoclay. *Chem Mater* **1999**, *11* (7), 1942-1947.
- 44 (20) Yeh, J. M.; Chen, C. L.; Huang, C. C.; Chang, F. C. Effect of organoclay on the thermal
- 45 stability, mechanical strength, and surface wettability of injection-molded ABS-clay
- 46 nanocomposite materials prepared by melt intercalation. *J Appl Polym Sci* **2006**, *99* (4), 1576-
- 47 1582.
- 48 (21) Li, C.; Wilkes, G. L. Silicone/amine resin hybrid materials as abrasion resistant coatings.
- 49 *Chem Mater* **2001**, *13* (10), 3663-3668.
- 50
- 51
- 52
- 53
- 54
- 55
- 56
- 57
- 58
- 59
- 60

- 1  
2  
3  
4  
5  
6  
7  
8  
9  
10  
11  
12  
13  
14  
15  
16  
17  
18  
19  
20  
21  
22  
23  
24  
25  
26  
27  
28  
29  
30  
31  
32  
33  
34  
35  
36  
37  
38  
39  
40  
41  
42  
43  
44  
45  
46  
47  
48  
49  
50  
51  
52  
53  
54  
55  
56  
57  
58  
59  
60
- (22) Lan, T.; Kaviratna, P. D.; Pinnavaia, T. J. On the nature of polyimide-clay hybrid composites. *Chem Mater* **1994**, *6* (5), 573-575.
  - (23) Gilman, J. W.; Jackson, C. L.; Morgan, A. B.; Harris, R. Flammability properties of polymerlayered- silicate nanocomposites: polypropylene and polystyrene nanocomposites. *Chem Mater* **2000**, *12* (7), 1866-1873.
  - (24) Yao, K. J.; Song, M.; Hourston, D. J.; Luo, D. Z. Polymer/layered clay nanocomposites: 2 polyurethane nanocomposites. *Polymer* **2002**, *43* (3), 1017-1020.
  - (25) Yeh, J. M.; Chen, C. L.; Chen, Y. C.; Ma, C. Y. Enhancement of corrosion protection effect of poly(o-ethoxyaniline) via the formation of poly(o-ethoxyaniline)-clay nanocomposite materials. *Polymer* **2002**, *43* (9), 2729-2736.
  - (26) Yeh, J. M.; Yu, M. Y.; Liou, S. J. Dehydration of water-alcohol mixtures by vapor permeation through PVA/clay nanocomposite membrane. *J Appl Polym Sci* **2003**, *89* (13), 3632-3638.
  - (27) Cho, M. S.; Choi, H. J.; Ahn, W. S. Enhanced electrorheology of conducting polyaniline confined in MCM-41 channels. *Langmuir* **2004**, *20* (1), 202-207.
  - (28) Yeh, J. M.; Liou, S. J.; Lai, C. Y.; Wu, P. C. Enhancement of corrosion protection effect in polyaniline via the formation of polyaniline-clay nanocomposite materials. *Chem Mater* **2001**, *13* (3), 1131-1136.
  - (29) Sridhar, L. N.; Gupta, R. K.; Bhardwaj, M. Barrier properties of polymer nanocomposites. *Ind Eng Chem Res* **2006**, *45* (25), 8282-8289.
  - (30) Bose, N. K.; Kamal, M. R. Influence of multiwall carbon nanotubes on the mechanical properties and unusual crystallization behavior in melt-mixed co-continuous blends of polyamide6 and acrylonitrile butadiene styrene. *Polym Eng Sci* **2009**, *49* (8), 1533-1543.
  - (31) Lee, C. H.; Kim, H. B.; Lim, S. T.; Choi, H. J. Biodegradable aliphatic polyester-poly (epichlorohydrin) blend/organoclay nanocomposites; synthesis and rheological characterization. *J Mater Sci* **2005**, *40* (15), 3981-3985.
  - (32) Maiti, M.; Bhattacharya, M.; Bhowmick, A. K. Elastomer nanocomposites. *Rubber Chem Technol* **2008**, *81* (3), 384-469.
  - (33) Bhattacharya, M.; Bhowmick, A. K. Polymer-filler interaction in nanocomposites: new interface area function to investigate swelling behavior and Young's modulus. *Polymer* **2008**, *49* (22), 4808-4818.
  - (34) Krook, M.; Albertsson, A. C.; Gedde, U. W.; Hedenqvist, M. S. Barrier and mechanical properties of montmorillonite/polyesteramide nanocomposites. *Polym. Eng. Sci.* **2002**, *42* (6), 1238-1246.
  - (35) Zhong, Y.; Janes, D.; Zheng, Y.; Hetzer, M.; Kee, D. D. Mechanical and oxygen barrier properties of organoclay-polyethylene nanocomposite films. *Polym. Eng. Sci.* **2007**, *47* (7), 1101-1107.
  - (36) Bharadwaj, R. K. Modeling the barrier properties of polymer-layered silicate nanocomposites. *Macromolecules* **2001**, *34* (26), 9189-9192.
  - (37) Drozdov, A. D.; Christiansen, J. D.; Gupta, R. K.; Shah, A. P. Model for anomalous moisture diffusion through a polymer-clay nanocomposite. *J. Polym. Sci. Part B: Polym. Phys.* **2003**, *41* (5), 476-492.
  - (38) Musto, P.; Mascia, L.; Mensiteri, G.; Ragosta, G. Diffusion of water and ammonia through polyimide-silica discontinuous nanocomposites: interactions and reactions. *Polymer* **2005**, *46* (12), 4492-4503.
  - (39) Vlasveld, D. P. N.; Groenewold, J.; Bersee, H. E. N.; Picken, S. J. Moisture absorption in polyamide-6 silicate nanocomposites and its influence on the mechanical properties. *Polymer* **2005**, *46* (26), 12567-12576.
  - (40) Shantalii, T. A.; Karpova, I. L.; Dragan, K. S.; Privalko, E. G.; Privalko, V. P. Synthesis and thermomechanical characterization of polyimides reinforced with the sol-gel derived nanoparticles. *Sci. Technol. Adv. Mater.* **2003**, *4* (2), 115-119.

- 1 (41) Pluart, L. L.; Duchet, J.; Sautereau, H. Epoxy/montmorillonite nanocomposites: influence of  
2 organophilic treatment on reactivity, morphology and fracture properties. *Polymer* **2005**, *46* (26),  
3 12267-12278.
- 4 (42) Akorna, G.; Ugi, I. Isocyanide Synthesis with Diphosgene. *Angew Chem Int Ed Engl* **1977**, *16*  
5 (4), 259-260.
- 6 (43) Nair, C. P. R.; Glouet, G.; Guilbert, Y. Flame and thermal resistance of phosphorus-  
7 functionalized poly(methyl methacrylate) and polystyrene. *Polym Degrad Stsb* **1989**, *26* (4),  
8 305-331.
- 9 (44) Yu, Y. H.; Jen, C. C.; Huang, H. Y.; Wu, P. C. Preparation and properties of heterocyclicly  
10 conjugated poly(3-hexylthiophene)-clay nanocomposite materials. *J Appl Polym Sci* **2004**, *91*  
11 (6), 3438-3446.
- 12 (45) Yeh, J. M.; Chin, C. P. Structure and properties of poly(o-methoxyaniline)-clay nanocomposite  
13 materials. *J Appl Polym Sci* **2003**, *88* (4), 1072-1080.
- 14 (46) Kornmann, X.; Lindberg, H.; Berglund, L. A. Synthesis of epoxy-clay nanocomposites:  
15 influence of the nature of the clay on structure. *Polymer* **2001**, *42* (4), 1303-1310.
- 16 (47) Kornmann, X.; Lindberg, H.; Berglund, L. A. Synthesis of epoxy-clay nanocomposites.  
17 influence of the nature of the curing agent on structure. *Polymer* **2001**, *42* (4), 4493-4499.
- 18 (48) Messersmith, P. B.; Giannelis, E. P. Synthesis and characterization of layered silicate-epoxy  
19 nanocomposites. *Chemistry of Materials* **1994**, *6* (10), 1719-1725.
- 20 (49) Katti, D. R.; Katti, K. S.; Shanmugasundaram, V. Role of clay-solvent inter and intraparticle  
21 interactions on swelling characteristics of montmorillonite nano-meso-micro scale particulate  
22 systems. *Mater. Res. Soc. Symp. Proc.* **2001**, *704*, 257-262.
- 23 (50) Wypych, F.; Schreiner, W. H.; Mattoso, N.; Mosca, D. H.; Marangoni, R.; Bento, C. A.  
24 Covalent grafting of phenylphosphonate groups onto layered silica derived from in situ-leached  
25 chrysotile fibers. *J. Mater. Chem.* **2003**, *13* (2), 304-307.
- 26 (51) Patel, H. A.; Somani, R. S.; Bajaj, H. C.; Jasra, R. V. Preparation and characterization of  
27 phosphonium montmorillonite with enhanced thermal stability. *Applied Clay Science* **2007**, *35*  
28 (3-4), 194-200.
- 29 (52) Miyagawa, H.; Mohanty, A.; Misra, M. Effect of clay and alumina-nanowhisker  
30 reinforcements on the mechanical properties of nanocomposites from bio-based epoxy: a  
31 comparative study. *Ind Eng Chem Res* **2004**, *43* (22), 7001-7009.
- 32 (53) Wang, L.; Wang, K.; Chen, L.; Zhang, Y.; He, C. Preparation, morphology and  
33 thermal/mechanical properties of epoxy/nanoclay composite. *Composites A* **2006**, *37* (11), 1890-  
34 1896.
- 35 (54) Benveniste, Y. A new approach to the application of Mori-Tanaka's theory in composite  
36 materials. *Mech Mater* **1987**, *6* (2), 147-157.
- 37 (55) Schjodt-Thomsen, J.; Pyrz, R. The Mori-Tanaka stiffness tensor: diagonal symmetry, complex  
38 fibre orientations and non-dilute volume fractions. *Mech Mater* **2001**, *33* (10), 531-544.
- 39 (56) Wu, T. T. The effect of inclusion shape on the elastic moduli of a two-phase material. *Int J*  
40 *Solids Struct* **1966**, *2* (1), 1-8.
- 41 (57) Wang, J.; Pyrz, R. Prediction of the overall moduli of layered silicate-reinforced  
42 nanocomposites part I: basic theory and formulas. *Compos Sci Technol* **2004**, *64* (7-8), 925-934.
- 43 (58) Wang, J.; Pyrz, R. Prediction of the overall moduli of layered silicate-reinforced  
44 nanocomposites - part II: analyses. *Compos Sci Technol* **2004**, *64* (7-8), 935-944.
- 45 (59) Kornmann, X.; Berglund, L. A.; Sterte, J.; Giannelis, E. P. Nanocomposites based on  
46 montmorillonite and unsaturated polyester. *Polymer Eng Sci* **1998**, *38* (8), 1351-1358.
- 47 (60) Wu, Z.; Zhou, C.; Qi, R.; Zhang, H. Synthesis and characterization of nylon 1012/clay  
48 nanocomposite. *J Appl Polym Sci* **2002**, *83* (11), 2403-2410.
- 49 (61) Tyan, H. L.; Wei, K. H.; Hsieh, T. E. Mechanical properties of clay-polyimide (BTDA-ODA)  
50 nanocomposites via ODA-modified organoclay. *J Polym Sci: Part B: Polym Phys* **2000**, *38* (22),  
51 2873- 2878.
- 52  
53  
54  
55  
56  
57  
58  
59  
60

- 1  
2  
3  
4  
5  
6  
7  
8  
9  
10  
11  
12  
13  
14  
15  
16  
17  
18  
19  
20  
21  
22  
23  
24  
25  
26  
27  
28  
29  
30  
31  
32  
33  
34  
35  
36  
37  
38  
39  
40  
41  
42  
43  
44  
45  
46  
47  
48  
49  
50  
51  
52  
53  
54  
55  
56  
57  
58  
59  
60
- (62) Crank, J. *The mathematics of diffusion*. Oxford **1956**, Clarendon.
- (63) Liu, W.; Hoa, S. V.; Pugh, M. Water uptake of epoxy-clay nanocomposites: Model development. *Compos Sci Technol* **2007**, *67* (1), 3308-3315.
- (64) Haq, M.; Burgueño, R. Modeling and simulation of bio-based polymer/clay nanocomposites through a multilevel FE approach. *Proceedings of sixth international conference on computation of shell & spatial structures* **2008**, New York, SessionT-2-E.



442x158mm (300 x 300 DPI)